Biomass-based photothermal materials for interfacial solar steam generation: A review

Idris Ibrahim[a], Vrushank Bhoopal[b], Dong Han Seo[a], Morteza Afsari[a], Ho Kyong Shon[a], Leonard D. Tijing[a*]

[a]Centre for Technology in Water and Wastewater, School of Civil and Environmental Engineering, University of Technology Sydney, PO Box 123, 15 Broadway, Sydney, NSW, 2007, Australia

[b]Faculty of Engineering and Information Technology, University of Technology Sydney, PO Box 123, 15 Broadway, Sydney, NSW, 2007, Australia

[*]Corresponding author: L.D. Tijing, email: leonard.tijing@uts.edu.au

Abstract

An efficient photothermal conversion process is essential for making high performing solar steam generation (SSG) device for water desalination and purification. Recently, biomass-based materials have attracted significant attention as useful substrates for SSG. This is attributed to their merits of biocompatibility, abundance, low thermal conductivity, and hydrophilicity. A deeper understanding of their various forms and structures and related photothermal conversion properties need further exploration to develop efficient and effective systems. This review discusses the photothermal conversion processes of biomass-based photothermal materials (BPTMs) for SSG, including their optical properties, capillary water action, and strategies for mitigating salt crystallization and fouling issues. The solar water evaporation performance and the current progress in utilizing BPTMs for water desalination and wastewater treatment applications are also discussed. This review will stimulate further investigation and research interest on the use of BPTMs from lab-scale to large-scale outdoor SSG applications. New insights on novel ideas for further development in biomass material-based SSG for water desalination are elucidated in this review.

Keywords: Biomass, photothermal conversion process, solar steam generation, water desalination

Highlights

- Review of using diverse biomass integrated photothermal materials.
- Factors affecting solar evaporation efficiencies and performance are discussed.
- Application of BPTMs in solar steam generation and solar desalination are illustrated.
- The current challenges and future research directions in the field are elucidated.

Contents

1. Introduction

Clean and safe water is essential for sustaining human lives on earth. Recent studies revealed that by 2025, almost three billion people would experience severe water shortages [1]. However, current technologies for desalination and water treatment, including reverse osmosis (RO) and multi-stage flash distillation (MSF), experience drawbacks such as high energy consumption (i.e., designed mainly for a large-scale operation), and environmental pollution [2]. It is estimated that producing 1,000 m^3/day of drinking water using the thermal desalination process consumes ~10,000 tons of oil per year [3]. Moreover, such high cost and energy requirements make it impractical for applying these technologies in rural areas where few people live, thus requiring low-energy consumption, and simple and effective solution [4, 5].

SSG devices have been reported as effective and promising solutions for clean water production [6-8]. The process is based on utilizing sunlight and photothermal materials (PTMs) to produce clean water providing a low-cost alternative approach for water supply especially in remote areas [9-12]. Solar steam generation (SSG) devices are simple in construction, portable, and can be used off-grid, making for facile implementation in the field. During the process, solar irradiation of 1 sun (~1 kW m^{-2}) is directly received by PTM or solar absorber, where photon energy is converted into thermal energy, to heat up the water underneath resulting in accelerated water evaporation [9, 11, 13].

The increasing development in nanomaterials and promising results in various fields such as dye-sensitized solar cells [14], photodetector [15], and photocatalyst [16] has attracted tremendous attention to applying this technology in SSG for water purifications applications. In the first study, Halas' demonstrated dispersed gold nanoparticles (NPs) system in SSG, where water vapor is generated through boiling mechanisms, achieving 80% efficiency [17]. Later on, Chen's group initiated a new approach to utilize heat and suppress the losses. They

separated the solar absorber part from the bulk water using a thermal insulator in a system called interfacial SSG [18]. Exfoliated graphite has used as a solar absorber coated on hydrophilic porous carbon foam (thermal insulator), which results in water evaporation efficiency of ~85%. Later on, a number of groups have tried to improve the efficiency of solar evaporator by using different solar absorbers and system designs.

To design a highly-efficient SSG system for desalination, it needs to satisfy four main criteria: (i) use of PTMs with excellent optical properties; (ii) the solar absorber (i.e., PTM and substrate) should have low thermal conductivity to localize the heat; (iii) the system should possess fast water transport channels [19-24], and; (iv) the absorber should exhibit anti-salt crystallization properties when evaporating saline feedwater [19, 25]. Recently, a wide range of PTMs/solar absorber was reported for strong light absorption, such as carbon-based materials [26-28], plasmonic metals [29], inorganic semiconductors nano/microstructure [30-33], and conjugated polymeric materials [34-36]. Besides the PTMs, investigating and improving of SSG devices components such as supporters, thermal insulators, and water capillary channels have been widely investigated.

In recent years, there has been increasing interest on the use of biomass-based materials (i.e., wood, bamboo, sugarcane, etc.) either as stand-alone solar absorber, or as substrate to other PTMs for SSG. Owing to their abundance in nature, hydrophilicity, low-cost, and environmentally-friendly, biomass-based materials have shown significant advantages in utilization as PTMs (see **Fig. 1**) [24, 37, 38]. Biomass-based PTMs (BPTMs) exhibit excellent thermal insulating properties (low thermal conductivity), and possess fast water transport channels (e.g., 1 mm high corn stalk exhibits transmission of water to top surface within ~2 s when in contact with water), which are desired features for highly efficient solar evaporator [39]. Some studies have also signified their self-cleaning capability, which is beneficial for combating salt formation during desalination via SSG. Despite these advantages, biomass

materials possess limited solar light absorption capacity. Hence, two main strategies were proposed to enhance the light absorption: (i) carbonization process, and (ii) integration with nanocomposite PTMs. Low-cost SSG devices can be built using BPTMs, which can be attractive for implementation in large-scale practical applications [40-45].

Recently, several review articles highlighted the many aspects of SSG process such as those focussing on PTM materials [46], heat management [19], anti-salt strategies [47], carbon materials [48, 49], graphene oxide [50], plasmonic metals [51], and general SSG systems [52]. However, there is still no critical review discussing the recent updates and future research directions on the working mechanism and the potentials applications of BPTMs in SSG.

However, to the best of our knowledge, no review has been reported yet on the applications of biomass-based photothermal materials (BPTMs) in SSG for desalination, which is ought to be elucidated. In this review, we discuss the up-to-date progress of BPTMs for clean water production, including details of the contribution of biomass materials for light absorption and photothermal conversion processes, thermal management, and water transport. We then evaluate the performance of BPTMs for water desalination and end our discussion with the conclusion, challenges and perspectives, providing further insight into the future research and development of BPTMs in SSG application.

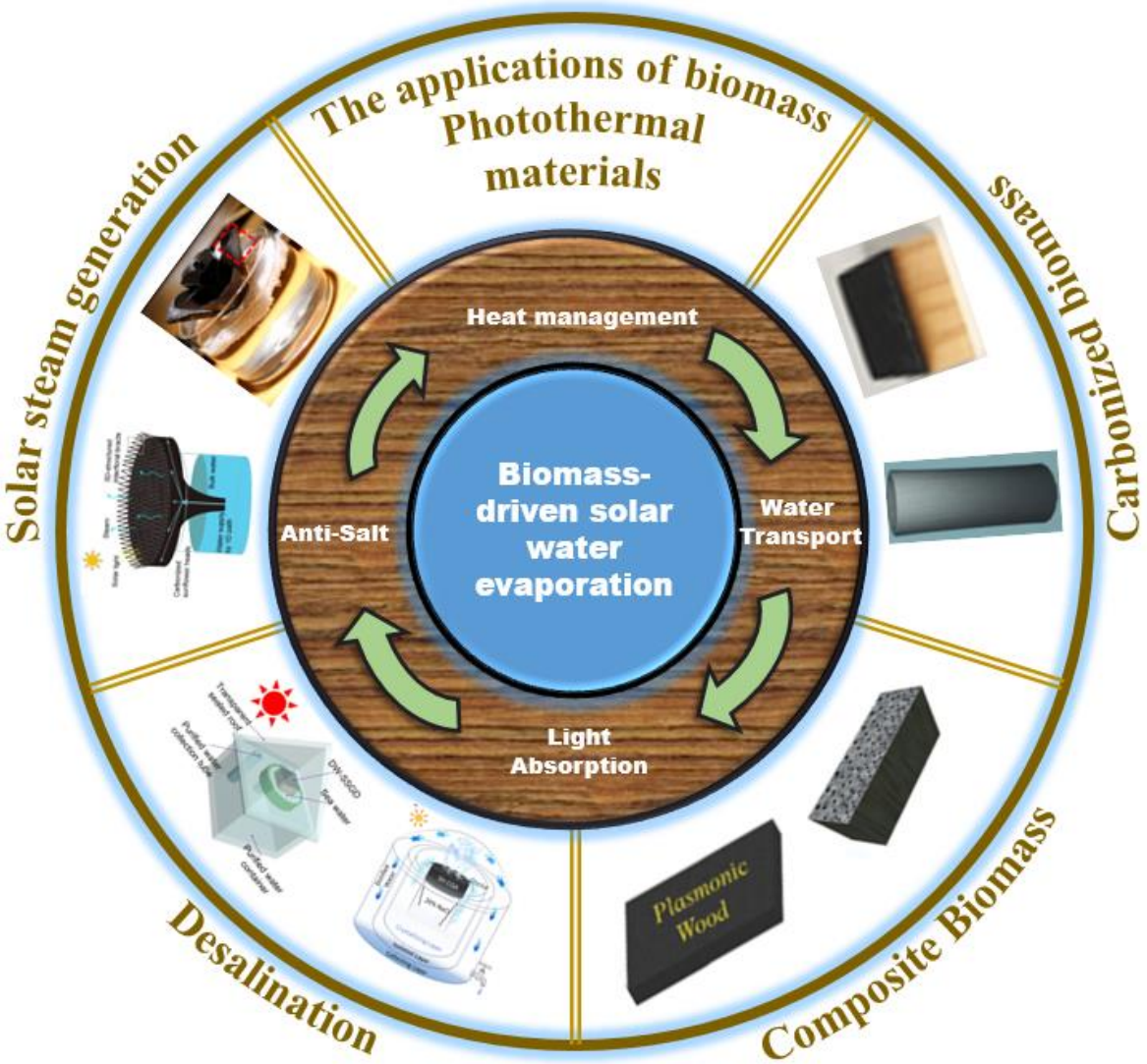

Fig. 1. Attractive characteristics of biomass-based photothermal materials for solar steam generation and their various applications.

2. The role of biomass surface functions for enhancing SSG performance

Biomass materials have the advantage of structural composition (e.g., porosity, rich microchannels), making them useful substrates that can be integrated with various nanostructure PTMs for high efficient SSG devices. The intrinsic features of BPTMs can lead to remarkable SSG performance with broadband light absorption across the whole solar spectrum, excellent heat management and utilization, fast and continuous water supply with anti-salt characterizations [49, 53]. **Fig. 2** illustrates the various features of biomass substrate in enhancing solar steam generation performance. Details of the contribution of bioinspired substrates in improving the overall SSG will be discussed in the next sections.

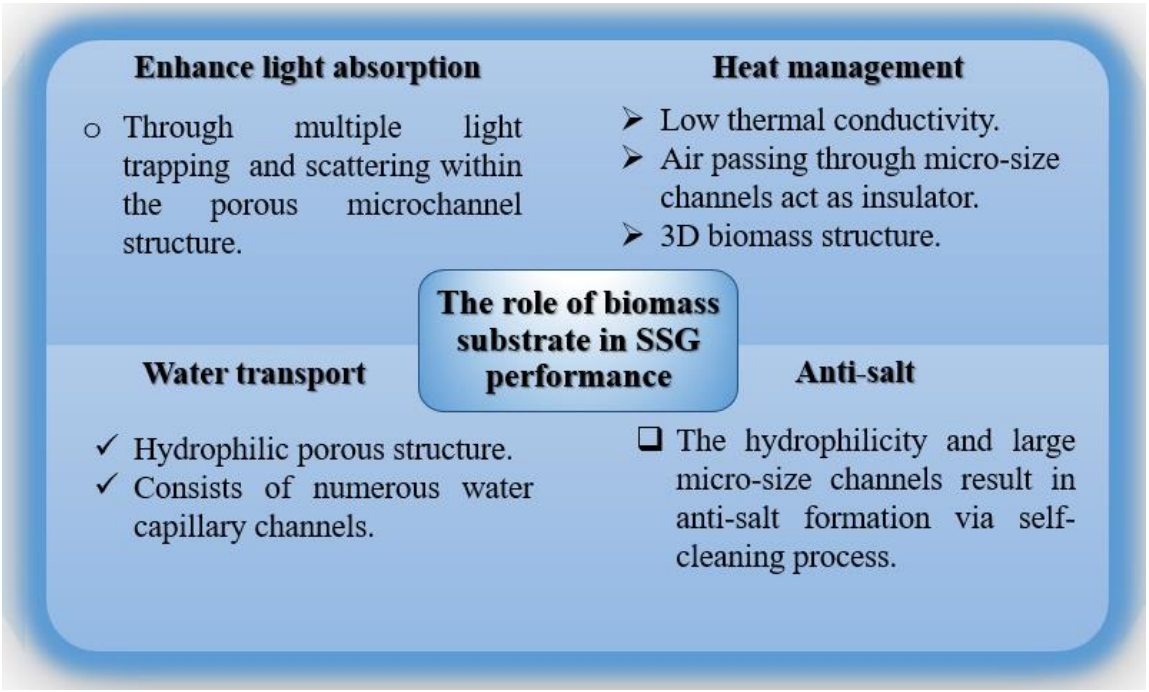

Fig. 2. Schematic illustration of the role of biomass in enhancing the SSG performance.

2.1 Boosting the light absorption characteristics

Light absorption characteristics of PTMs play a critical role in photothermal conversion efficiency in SSG [9]. An ideal PTM should be able to absorb sunlight over the whole solar

157 spectrum (wavelength from 250-2500 nm): ultraviolet region (UV), visible region (vis), and
158 the near-infrared region (NIR) (see **Fig. 3a**) [19, 54, 55]. Biomass substrates exhibit high
159 porosity and open microchannel, which act as a good substrate for enhancing the light
160 absorption of PTMs. Intrinsic micropores and 3D microstructures can enable multiple sunlight
161 scattering and trapping through the pore vessels, leading to sunlight absorption covering the
162 solar spectrum, however still with an insufficient capacity [56]. The incorporation of nanoscale
163 sizes PTM into a biomass structure can maintain the microporosity of the biomass substrate
164 while helping in internal light trapping and reflection thereby broadening the light absorption.
165 For example, in the case of plasmonic metals, researchers proposed different strategies to
166 extend the light absorption by regulating their size and morphology [57], or through
167 incorporation with porous substrates (e.g., anodized alumina oxide (AAO) [57], electrospun
168 polyvinylidene fluoride (PVDF) [58], phase inversion PVDF [59], and filter paper [57], *etc.*).
169 However, the light absorption efficiency was mostly limited to the UV-Vis region, and
170 extending the light absorption to the NIR region was often challenging. Such limitation can be
171 overcome using biomass substrates through the abundance of internal meso/micropores,
172 allowing multiple light reflection and scattering that occur within the pathways [60]. Formation
173 of such composite material of plasmonic metal-biomass-based materials leads to more
174 broadband light absorption across the entire solar spectrum (UV-vis-NIR). Such a result
175 motivated researcher to apply various approaches to improve the light absorption
176 characteristics. For instance, plasmonic Pd NPs decorated on a wood prepared by a simple
177 coating process exhibited light absorption beyond the UV-vis region [60]. The fabrication of
178 plasmonic wood with the light absorption and vapor transport mechanism is given in **Fig. 3c**.
179 The result showed excellent light absorption (~99%) across the UV-vis-NIR region. A similar
180 approach could be applied using different NPs. For example, polypyrrole NPs exhibited a light
181 absorption of 90.8% across the solar spectrum. After incorporating into the wood's

microchannels, the light absorption increased to 97.5% as attributed to the synergistic effect [42]. Aside from using biomass as substrates for PTM, an integrated system wherein the top surface of the biomass is carbonized, acting as the solar absorber, while the non-carbonized part serves as the support and wicking channels [56, 61, 62]. This process turns the color of biomass into black and increases the ratio of π-conjugated bonds, hence excellent optical characteristic is obtained [63]. For example, Qiu et al. described the importance of regulating the surface area and pore size of carbon foam derived from carbonized wood to boost the light absorption [64]. In their study, 3D interconnected carbon foam was designed with the rough surface via alkali treatment with varying KOH concentrations (2 g (CF-1), 5 g (CF-2), and 10 g (CF-3)) (refer to **Table 1**). As revealed in **Fig. 3b**, with an increase in pore size and surface area, the light absorption was further increased. CF-3 displayed the highest optical absorption of 97% over the whole solar spectrum. This is attributed to surface roughness and enlarged pore structure, allowing light trapping to occur in the structure. Upon 1 sun illumination, SSG efficiency of 80.1% was obtained. Natural wood is reported to possess light absorption of 38.3% across the entire solar spectrum, and significant increase in light absorption is observed (~90%) after direct carbonizeation [64].

Table 1. BET surface area, pore-volume, and size of alkali-treated carbonized wood [64]

Materials	**Surface area ($m^2 g^{-1}$)**	**Pore Volume ($cm^3 g^{-1}$)**	**Average pore size (nm)**	**Light absorption (UV-vis-NIR)**
Wood	4.56	0.019	4.08	38.3
*CB	17.40	0.038	11.07	90.5
CF-1	22.45	0.40	15.91	NG
CF-2	28.32	0.051	26.00	NG
CF-3	36.76	0.064	47.99	97.2 (highest)

* CB: Carbon Black, NG: Not Given

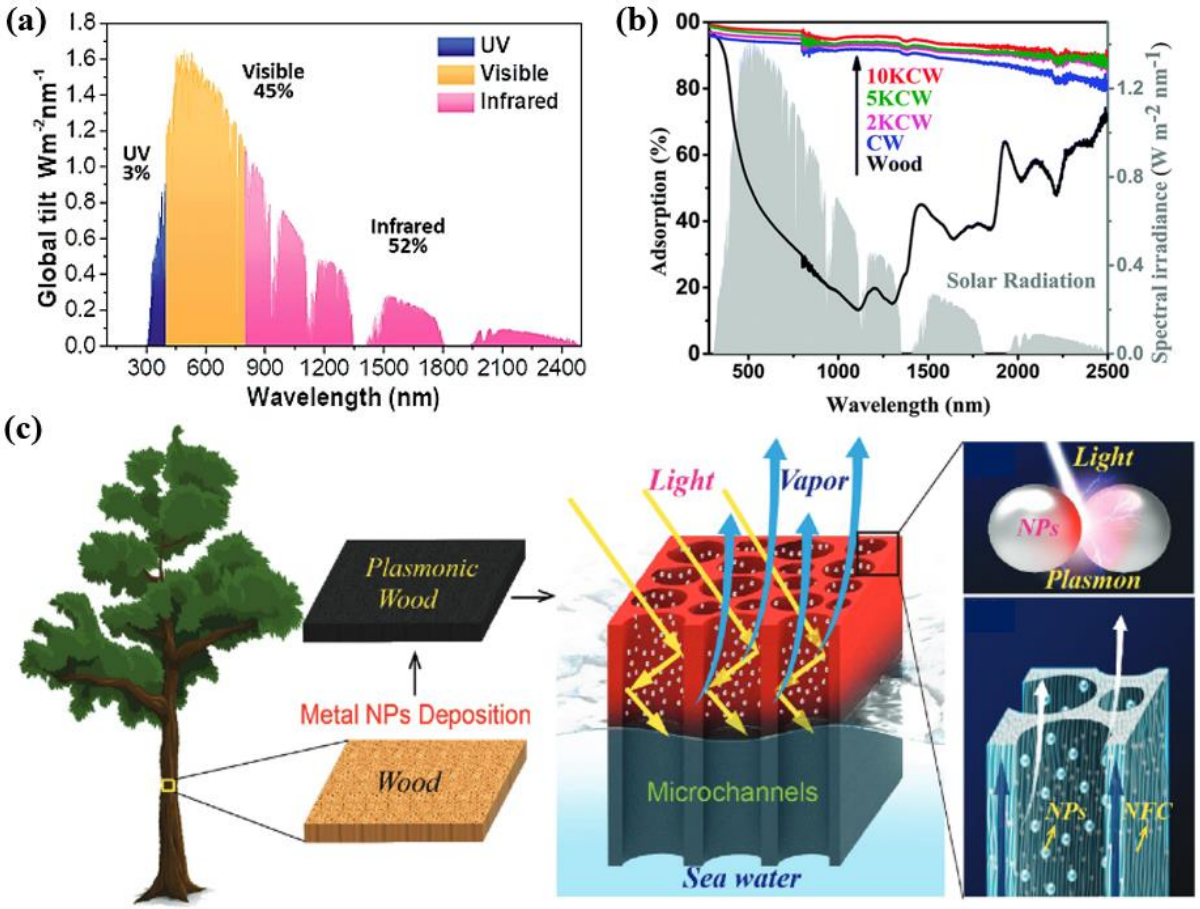

Fig. 3. (a) Solar spectral irradiance (AM 1.G) [65]. (b) The light absorption of carbonized biomass with different pores and surface area [64]. (c) Fabrication process of Pd NPs/Wood, after the plasmonic metal NPs deposition, light can pass into the wood vessels and be fully utilized for vapor generation, Image on the right display plasmonic effect of two adjacent metal NPs [60].

2.2 Strategies for suppressing the heat loss in BPTM systems

Thermal management is a crucial factor that influences the photothermal conversion efficiency in SSG. The efficiency of the SSG devices is directly proportional to the light-to-heat conversion efficiency of the absorber surface [18, 46]. It is essential to have a substrate that possesses good heat localization ability and restricts heat flow to the bulk water. Typically, by limiting the heat transmittance to the bulk water and surrounding areas, a large amount of heat can be localized, thus enabling the absorbed sunlight to be utilized and heat up the water layer [66].

The converted heat to energy must be fully utilized for excellent water evaporation performance. The heat losses in interfacial BPTMs must be suppressed and used, which can be done in three ways: (a) reduce the downward heat loss to the bulk water; (b) prevent heat loss to the surroundings, and; (c) maintaining the lower temperature at the solar absorber part compared to the surroundings for gaining energy from the environment (mainly achieved via 3D structure BPTM design) [52, 63, 67]. One of the commonly used strategies to induce heat localization and minimize conduction heat transmission to the bulk water is by introducing thermal insulators (e.g., polystyrene (PS) and expandable polyethylene (EPE), etc.) between the solar absorber and bulk water. **Fig. 4a** describes the heat transfer mechanism in SSG. However, most of the polymeric thermal insulators used are non-environmentally friendly [68]. Further, additional water capillary channels are essentially required due to its hydrophobicity.

Considerable efforts have been devoted to hunting effective solutions. For example, the capability of porous materials such as graphene foams to localize heat during water evaporation has been suggested [64]. Nonetheless, the complicated and expensive fabrication process limits its practical application. Therefore, research effort is directed to find a green method and low-cost material with low thermal conductivity and open multichannel for water transport. Hydrophilic biomass materials were found to be one of the best candidates. Numerous types of biomass materials were proposed as effective for heat localization and utilization, including wood (0.11-0.34 W m^{-1} K^{-1}) [38], bamboo (0.30 W m^{-1} K^{-1}) [38], sugarcane (0.08 W m^{-1} K^{-1}) [69], cotton (0.04 W m^{-1} K^{-1}), rice culm (0.5 W m^{-1} K^{-1}) [61], and daikon (0.04 W m^{-1} K^{-1}) [62]. Mesoporous biomass, such as wood, exhibits excellent thermal insulation for heat localization [43]. This is attributed to the pore microchannels in wood that allow the air from the outer environment to serve as a heat insulator via access to and travel along water vapor. Liu et al. demonstrated a versatile strategy to reduce heat losses by designing carbonized longitudinal wood (LW) composed of a top-layer of carbonized wood acting as a solar absorber, and bottom

side consisting of natural wood. For comparison, carbonized horizontal wood (HW) was also prepared [70]. The thermal conductivity of the entire system in LW was 0.11 W m^{-1} K^{-1}, which is relevantly lower than that of HW (0.34 W m^{-1} K^{-1}). This is ascribed to the low liquid loading resulting in more air passage through the microchannels contributing to heat localization (**Fig. 4c**). After 10 sun illumination, the solar conversion efficiency of 89% was obtained. Bamboo is another biomass-based material that possesses low thermal conductivity along the vessel, assisting in accumulating heat and suppressing the heat loss without any effect on the water evaporation performance [38]. Due to the low thermal conductivity of bamboo, high water evaporation efficiency was achieved. Liu et al. reported surface carbonized sugarcane exhibiting light absorption of ~ 98% across the entire solar spectrum [69]. Low thermal conductivity (0.08 W m^{-1} K^{-1}) was obtained due to the abundance of closed champers, thus providing excellent insulating properties and minimizing heat loss. Meanwhile, the presence of bundles of vertical channels enables water transport. All these factors lead to an SSG efficiency of 87.4% at 1 sun illumination. Similar to bamboo, its low thermal conductivity assisted the heat localization and enhanced the water evaporation to obtain high photothermal conversion efficiency of 87.4% at 1 sun irradiation [69]. Biomass-based materials with unique internal structure such as lotus seedpods, which consist of hierarchical macro/mesopore structures, after carbonization process exhibits low thermal conductivity of 0.079 W m^{-1} K^{-1}. Such property helps to reduce heat conduction to the bulk water [68]. The pore structure of biomass-based materials plays a significant role in adjusting the convection and radiation heat losses due to the large effective surface area for heat exchange [68]. In addition to that, the hydrophilicity allows rapid and continuous water supply from the bulk to upward through the microchannels. This phenomenon leads to making it act as a heat-insulating layer. Li et al. reported polypyrrole-corn straw (PCS) with alkali-treated (PCSA) and microwave alkali treatment (P-CSMA) foams. The pore sizes of PCSA 30-200 μm and PCSAM were 30-1000

μm corresponding to a low thermal conductivity at dry states of 0.022 W m^{-1} K^{-1} and 0.027 W m^{-1} K^{-1}, respectively [44]. The low thermal conductivity results in significant heat localization to confine the converted heat at the interface region and minimized the transmitted heat. Therefore, after solar irradiation of 1 sun, solar steam generation efficiency and evaporation rate of (89.74% and 1.67 kg m^{-2} h^{-1} for CSA) and (96.8% and 1.77 kg m^{-2} h^{-1} for CSMA) were obtained, respectively. The higher water evaporation rate of CSMA was due to the large pores of CSMA (~1 mm) compared to CSA. Recently, biomass driven-aerogel was demonstrated to have efficient thermal insulating properties compared to various biomass substrate such as wood [71]. For example, Zhang et al. reported ultralight, flexible, and bendable Au-GO aerogel as an effective method for excellent SSG [71]. The as-designed aerogel exhibited thermal conductivity ~0.0418 W m^{-1} K^{-1} and 0.0617 W m^{-1} K^{-1} at dry and wet states, respectively. Surprisingly, this reported value is much lower than natural wood or cotton, which reveals its excellent thermal insulating properties. Given this feature resulted in localizing heat at the evaporator and avoided any downward heat loss to the bulk water. The as-designed materials display evaporation rate and efficiency of 90.1% and 1.39 kg m^{-2} h^{-1}, respectively under 1 sun illumination.

Apart from the above-mentioned reports, designing 3D-structured biomass such as 3D carbonized bamboo and carbonized sunflower heads have been reported as effective tools for reducing and recovering heat losses. This unique design can recover energy loss caused by reflection and radiation heat released from the solar absorber part. The energy from the environment can be harvested for promoting water evaporation efficiency. It takes place through heat exchange between the temperatures of the side of the solar absorber with the lower temperature of the warmer environment [63, 72]. In a unique application of this concept, Sun et al. reported a 3D macroscopic shape of carbonized sunflower heads that can efficiently recover the heat lost via cavity (**Fig. 4b**) [73]. They realized that the bulk temperature remains

unchanged. The highest temperature occurred at the top surface at the central part of the receptacle (45 ^{o}C) and the lowest at the edge of receptal. Because of the excellent thermal insulating properties and capability to recover the heat loss of the disk-shaped receptacle, an outstanding SSG efficiency of 100.4% was achieved. This value is beyond the theoretical limit (100% solar conversion efficiency under 1 sun irradiation). 3D solar steam generators are intensely studied recently due to their outstanding performance, and this provides a potential solution to suppress heat losses and harvest energy from the environment. Efforts towards exploring various 3D designs of biomass substrate may open new opportunities for effective heat localization and conversion. In addition to that, biomass hydrogel displays excellent thermal insulating properties with low thermal conductivity values, which is much lower than diverse reported substrates.

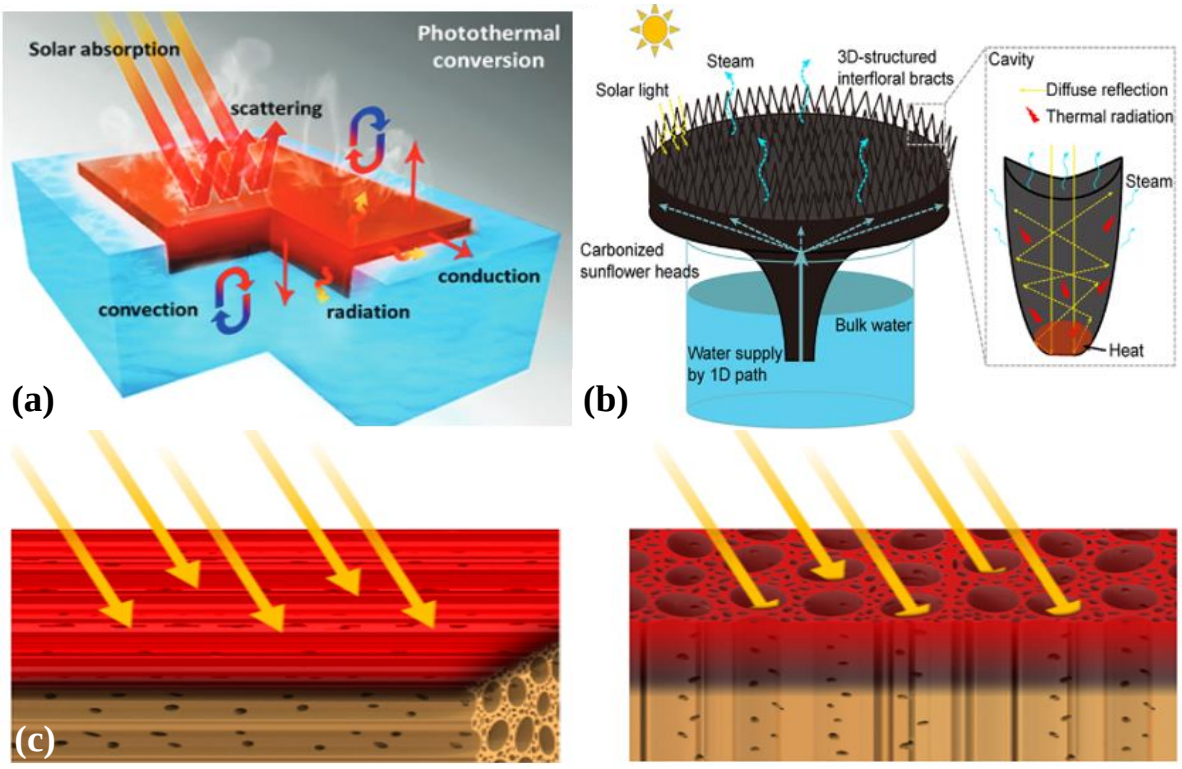

Fig. 4. Thermal management in photothermal biomass. (a) Schematic drawing of the photothermal conversion process for solar steam generation devices [65]. (b) Schematic of a carbonized sunflower head-based evaporator and a cavity [73]. (c) Schematic illustration of

heat localization on the carbonized longitudinal wood surface (left) and carbonized horizontal wood surface (right) [70].

2.3 Fast water transport

The water supply from the bulk water to upper part of the solar absorber region through capillary actions is a core component for highly efficient interfacial SSG systems. Biomass-based materials are made of hydrophilic cellulose with numerous micro/nanochannels, which are very helpful for efficient water transport, enabling high water evaporation efficiency [74, 75]. The process of transporting water in biomass is known as the transpiration process. It is inspired by the fact that trees can absorb water from the ground and deliver the water up to 100 m in height [60]. Other intrinsic features are self-floating properties without additional supporters. The water transport mechanism of the biomass is classified into three categories: 1D, 2D, and 3D pathway, depending on the structural features and the composition of the biomass. The 1D water channel was employed as a powerful strategy for continuous water transport from bulk water to the evaporation solar absorber region. The rich hydroxyl groups in the glucose, one of the main constituents in the biomass lead to highly hydrophilic channels. Numerous biomass materials were reported to exhibit a 1D water channel, including; cotton [36], mushrooms [76], lotus seedpods [68], and sunflower heads [73]. For instance, Xu's group et al. employed a cotton rod as a 1D water channel that could transport water to the solar absorber area of stackable nickel-cobalt/polydopamine sponge was separated from the bulk water. A remarkable water evaporation rate of 2.4 kg/m^2h was achieved (1 sun irradiation) [77]. Some parts in the biomass substrates possess 1D channel that can enable water transport. Carbonized mushrooms with umbrella-shaped maintain their hydrophilicity before and after the carbonization process [76]. This is attributed to its main components: carbohydrates, proteins, and some of the nitrogen functional groups that remain after the carbonization. The channel-tail (at the bottom of the mushroom) acts as water capillary channels. The heat loss in

the system was also suppressed, resulting in the solar conversion efficiency of 78% at 1 sun illumination. In contrast, carbonized sunflower heads having microchannel vascular bundles (diameter ~10-40 μm) aligned in a parallel direction provide a way for fast water transport. Other examples, such as carbonized lotus seed pods, containing numerous mesopore and macropore structures, also exhibited rapid water transport due to the strong water absorption from the bottom of the lotus petiole to the top surface (**Fig. 5d**) [68]. 2D channel is another type of water channel design by wrapping thermal insulator with hydrophilic cellulose-based material [78]. This design enables effective water transport to the top solar absorber layer via a 2D water path formed within the cellulose by a capillary force. For instance, Li et al. demonstrated polystyrene foam wrapped with cellulose to achieve 2D water transport from the bulk water to the graphene oxide film (solar absorber layer) [78]. 3D channels can also supply efficient water in interfacial SSG such as hydrophilic wood with 3D mesoporous structure, with numerous and highly aligned open micro/nanochannels for water transport. For example, the long vessel pore channels with a diameter of 50−100 μm in the flame treated wood can continuously pump water resulting to a water efficiency of 72%. Recently, it has been reported that manipulating the biomass surface or inducing a change in the biomass structure can endow materials with some extraordinary functions that can enhance water transport. For instance, Hu's group reported an artificial tree with a reverse-tree design. The structure allowed the water to pass in a direction perpendicular to what occurs in a natural tree that enhanced the water transport in the SSG device [70]. Chen et al. demonstrated an effective surface modification of biomass to improve water transport by removing hydrophobic lignin from the bulk wood using low-cost and environmentally friendly deep eutectic solvent (DES), as illustrated in **Fig. 5c** [79]. Meanwhile, the hydrophilic cellulose and hemicellulose remained on the bulk wood. The partial entrance of DES into the wood's cell walls formed hydrogen bonds, acting as glue to enhance mechanical stability. The SEM analysis revealed that the wood's structural

morphology remained unchanged with a tubular channel diameter of 20-80 μm. This modification method results in a water evaporation rate of 1.3 kg m^{-2} h^{-1} under 1 sun solar illumination. Despite the advantages of wood being a great material for efficient water transport, the lateral organization of wood however affects the water transport of saline water compared to other biomass with a non-lateral organization composed of vertical orientation. For example, bamboo exhibits open and vertically oriented water transport channel that facilitates rapid water transport compared to the one with lateral organization (**Fig. 5b**) [38]. Fang et al. demonstrated a full biomass-based SSG device that were made from wasted rice straw [61]. The upper leaves of rice straw were carbonized and used as a solar absorber. Meanwhile, the culms layout was utilized as water transport channels (length ~2 cm), as shown in **Fig. 5a**. The unique capillary structures and multilevel geometrical structures of the rice culms facilitated the efficient water transport to the carbonized upper leaf region which acted as a solar absorber. They realized that the 3D vertically aligned water channels facilitate water transport to the solar absorber region within 10 s, while 2D cellulose membrane (diameter 5 cm) exhibited fast water transport in 30 s. This leads to water evaporation rate and efficiency of 1.2 kg m^{-2} h^{-1} and 75.8%, respectively, achieved under 1 sun illumination.

Other biomass materials such as corn contain a vascular bundle with a diameter of 1.5 μm and abundant porous tissues. They exhibit superhydrophilic characteristics that are very beneficial for fast water capillary action [39]. The surface is fully covered within ~2 s with water inside the corn stalk at the height of 1 mm. The water transportation rate of this class of biomass is ten times higher than that of wood (**Fig. 5e**). PTM multi-walled carbon nanotubes and titanium dioxide were coated and used as PTM. A high-water evaporation rate of 2.48 kg m^{-2} h^{-1} and an efficiency of 68.2% were obtained (1 sun illumination). The water transport channel of biomass is highlighted in **Table 2.** Biomass materials display remarkable water transport making it promising for highly efficient SSG. The discovery of other biomass

substrates with unique transport channels to enhance and speed up water transport is worth exploring. Also, in carbonized biomass, more research is required to know the degree of carbonization effect on water transport. The modifications of biomass substrates are also needed for further modifying the pore vessels.

Table 2. Water transport channels in biomass-based material PTMs

Biomass source	Water evaporation channels	Ref
Wood	Porous microchannel	[60]
Bamboo	Non-lateral organization of porous and oriented microchannel	[38]
Cotton	Yarns under the force of pressure	[29]
Sugarcane	Vascular bundle	[69]
Corn stalk	Vascular bundle	[39]
Mushroom	Fibrous stipe	[76]
Carbonized sunflower head	Stalk	[73]
Carbonized daikon	Numerous interconnected channels	[62]
Rice straw	Culms	[61]

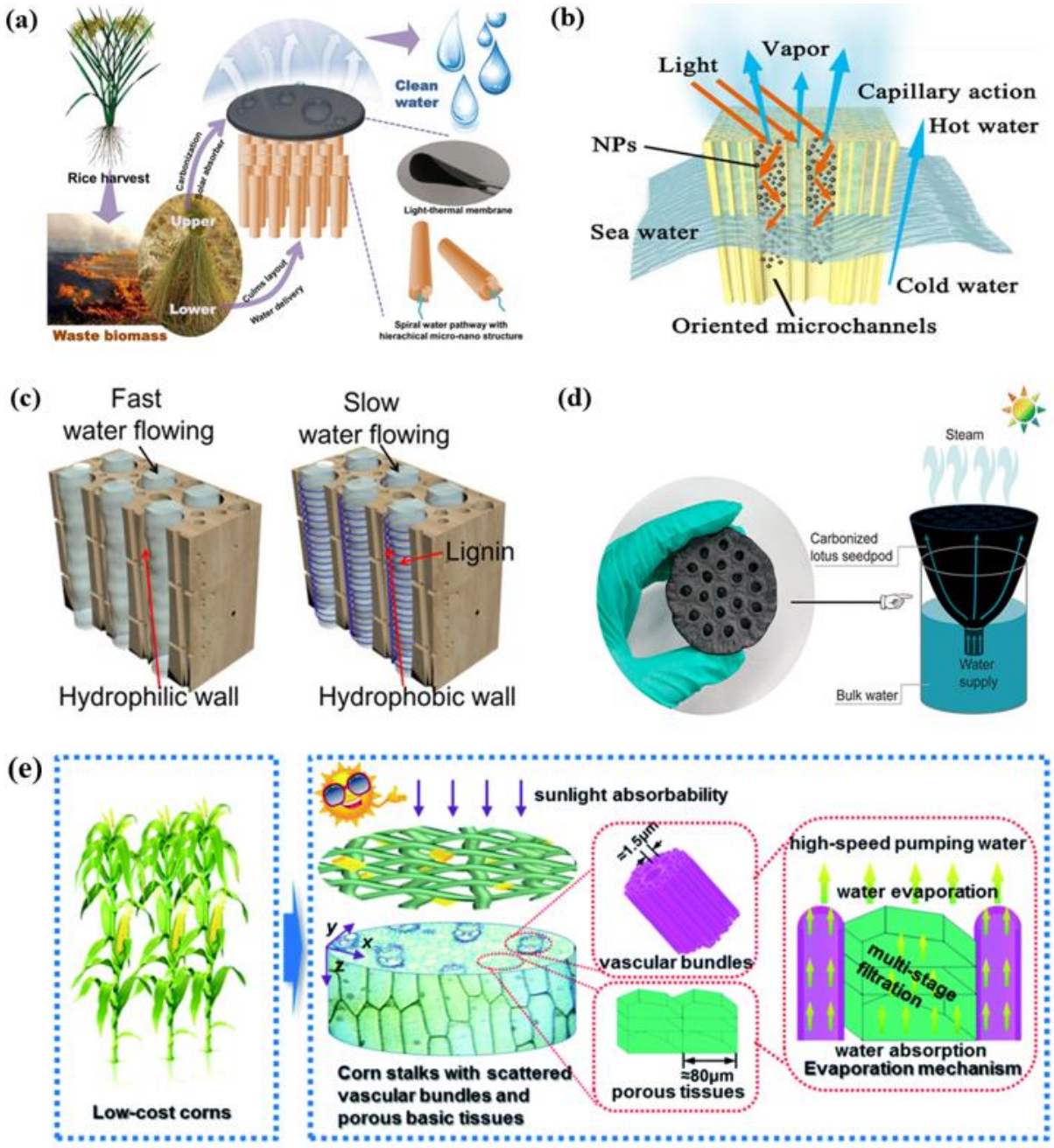

Fig. 5. Water pathway channel. (a). Illustration of rice straw driven solar evaporator [61]. (b) Capillary action of plasmonic NPs bamboo-composite PTM [38]. (c) Schematic of solar water evaporation of carbonized lotus seed. (d) Schematic of solar water evaporation of carbonized lotus seed [68]. (e) Water molecule transportation mechanism of natural corn stalks based solar evaporator system [39].

2.4 Anti-salt crystallization and self-cleaning capability

Salt crystallization is one of the main issues in water desalination for SSG. Therefore, it is essential to prevent or minimize it to allow the reusability and stability of the as-designed devices. The salt crystallization takes place when the water travels towards the PTMs and its supporting structures. The salt ions can migrate along with vapor and crystalize on the solar absorber layer [80]. The accumulation of salts on the solar absorber will have a detrimental effect on water evaporation especially when a high concentration of salts are crystallized. This leads to dramatically low photothermal conversion and water evaporation efficiency [81-84]. As a result, numerous methods have been proposed to enable anti-salt crystallization capability for the solar absorber system, and distinct improvements have been achieved. This includes coating the solar absorber with a superhydrophobic layer [85, 86], fabricating a Janus type membrane [5, 41, 87, 88], and using hydrophilic porous polymer architecture [2, 83]. The as-mentioned anti-salt methods tend to be unsatisfied due to the complicated process and instability of the process. In recent studies, biomass substrates have been suggested as an efficient substrate to mitigate salt accumulation. This happens through self-cleaning via the hydrophilic porous microchannels with a large diameter, allowing continuous water evaporation and dissolution of the formed salt to the bulk water [80, 89, 90]. **Table 3** presents the numerous methods proposed in literature to enable anti-salt crystallization capability for the solar absorber system. For instance, He et al. investigated the anti-salt crystallization of bimodal porous balsa wood and found it to lessen salt crystallization and maintained a stable water evaporation rate [81]. As revealed in **Fig. 6b**, the brine solution diffuses to the large vessel channel surroundings, which contributes to salt exchange with the brine bulk. Such a salt exchange process can effectively prevent salt crystallization and accumulation in the solar absorber region. To prove the phenomena of vessel channel contribution on the anti-crystallization, they conducted additional experiments by blocking the vessel channel with

polydimethylsiloxane (PDMS). The results revealed that there was salt accumulation on the surface when one channel was blocked, as shown in **Fig. 6c**, confirming the vital role of the vessel channel in anti-salt crystallization.

Recently, Li et al. reported a unique device to alleviate salt crystallization issues while enabling fast water transport [80]. As described in **Fig. 6a**, the device consists of carbonized green algae as a solar absorber with added cotton thread as an anti-salt crystallizer. During the evaporation process, they observed that salt crystallization took place in the cotton thread regions rather than the carbonized algae region. This can be explained by the stronger adhesion of salts on cotton threads than cohesion, as illustrated in **Fig. 6a**. Additionally, the cotton-aided device plays a significant role as anti-salt crystallization as no salt is observed on the solar absorber part for up to 15 days of operation. The biomass-driven hydrogel also displayed high resistance against salt crystallization formation after placing the NaCl solution for 30 mins [91]. The self-cleaning function in hydrogel-based PTM occurs through an equilibrium established by water transport-induced salt ion absorption and diffusion-enabled salt ion discharge processes [91]. Bian et al. examined the long term anti-salt tolerance of 3D carbonized bamboo by placing the BPTM under light illumination for 16 hours [92]. After the light irradiation, they noticed salt crystallization on the outer and inner surface of the carbonized bamboo. With continuous water evaporation, the crystallized salts were dissolved, demonstrating its self-cleaning ability.

The studies mentioned above reveal that biomass-based materials exhibit excellent resistance against salt crystallization through unique internal structures. The exploration of different anti-salt crystallization effects induced by various biomass-based materials is required. Simulation techniques such as molecular dynamics simulation could be very useful in understanding water diffusion and the salt exchange process thoroughly. This is necessary to design a good device for solar desalination.

458

459 **Table 3.** Comparison of strategies used for anti-salt crystallization in solar steam generation.

Classifications	Process	Drawbacks	Ref
Janus membranes	Combination of hydrophobic layer as salt resistant, and bottom hydrophilic layer for water transport	The combinations of two layers are complicated and instable process	[25, 87, 88]
Coating hydrophobic surface layer	Through spray coating or vacuum depositions with silane layer on hydrophilic PTM	Physical interactions of silane with PTM result instability issues	[85, 93]
Porous polymer structures	Superhydrophilicity and macroporous structure, a fast dissolution of salt which may crystallize within pores of materials and transfer back to saline solution could be achieved	Complicating fabrication process	[2, 83, 94]
	Introduction of ionic liquid moiety caused repulsion effect on cations in salt solution and has a salt resistant capability	More research investigations are required	[2, 94]
Natural Biomass	Hydrophilic biomass substrate composed of micro-aligned channels contributing in self-cleaning of accumulated salt	-	[80, 81, 91, 92]

460

461

462

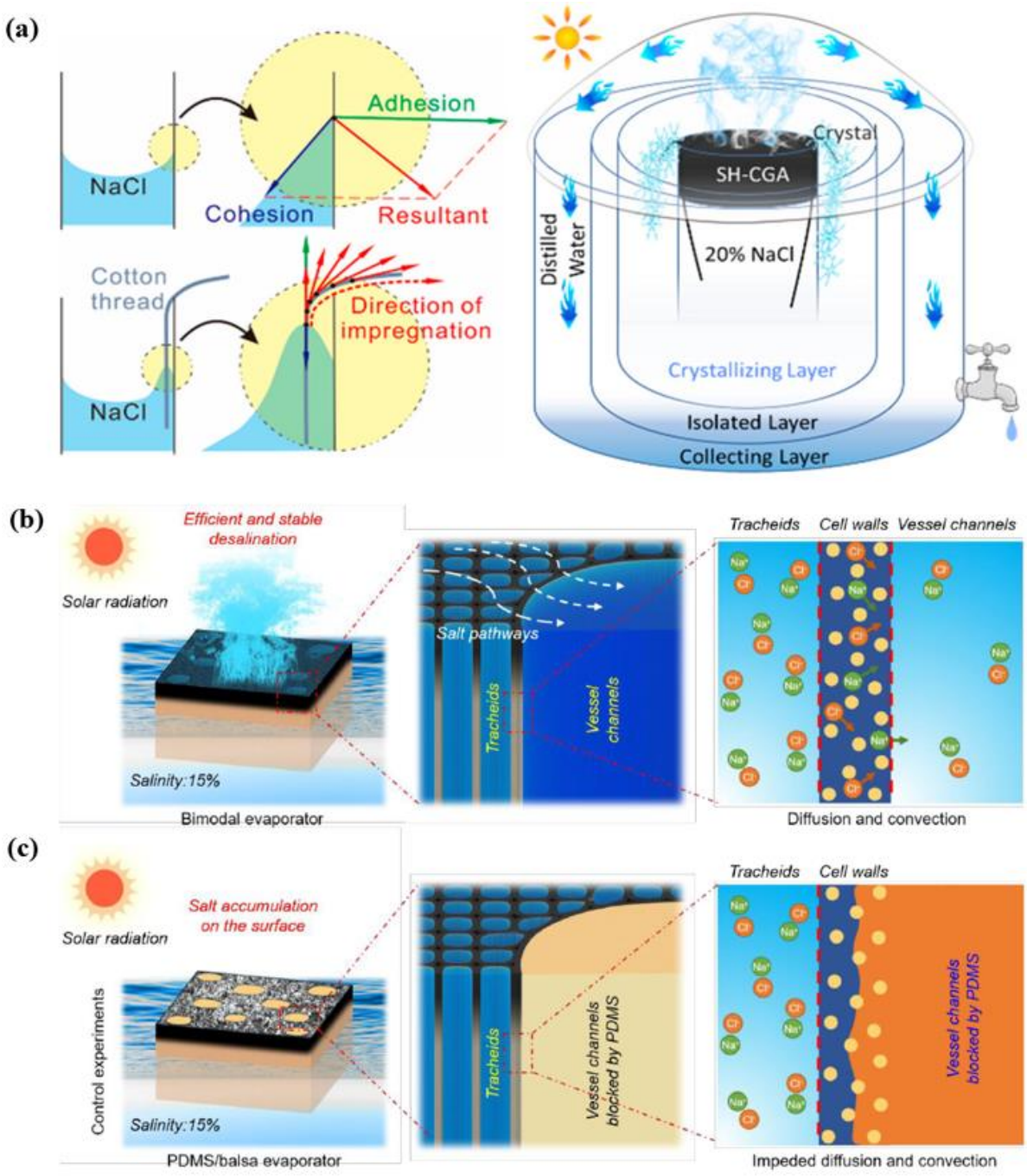

Fig. 6. Anti-salt accumulation and crystallization. (a) Schematic illustration of the ionic composition of simulated seawater and distilled water form superhydrophilic carbonized green algae [80]. (b),(c) Schematic illustrating the working principle of the bimodal porous balsa wood for anti-salt crystallization and fouling mechanism [81].

3. Solar steam generation performances of various BPTMs

To evaluate the water evaporation performance of BPTMs, indoor experiments are first conducted to determine the water evaporation rate and the efficiency under controlled solar illumination. The temperature of the evaporation area is usually visualized using an infrared camera. The weight change is measured using an electronic balance.

3.1 Carbonized biomass-based PTMs

Carbonization of biomass-based materials via a one-step pyrolysis process at high temperatures is one of the most common strategies to improve the solar absorption of biomass materials. This can be obtained through partial carbonization of the top part of biomass or carbonization of the whole biomass structure. Early studies demonstrated the use of carbonized wood as a PTM for high-efficiency solar steam generation devices due to its natural hydrophilicity and porous microchannels that facilitate water transport and its excellent thermal insulation properties. In 2017, Jia et al. conducted an intensive study on using different kinds of wood (e.g., pine, cocobolo, and padauk wood) as PTMs [95]. The wood was partially carbonized at 500 ^{o}C using a hot plate. **Fig. 7c** reveals the light absorption characteristics of poplar, pine, and cocobolo wood (92%, 84%, and 96%), respectively. Due to the high porosity of poplar wood, it obtained the highest water evaporation rate. The thermal conductivity was measured using a reverse wood (R-wood) configuration and a longitude wood (L-wood) configuration. The result showed thermal conductivities at dry state (L-wood configuration) of 0.27, 0.32, and 0.34 W m^{-1} K^{-1} for poplar, pine and cocobolo wood, respectively. Whereas, at R wood configuration, the thermal conductivities at dry state were 0.12, 0.14, and 0.21 W m^{-1} K^{-1}, respectively. As shown in **Fig. 7a**, such a result reveals that the wood vessels' orientation and its channel have a significant influence when using wood as a PTM. The light-to-heat conversion process in various woods was demonstrated by visualizing the surface heat distribution using an infrared

camera. The temperature gradient across the carbonized wood revealed that the temperature change in R-wood was higher than that of L-Wood configuration (**Fig. 7b**). At 10 sun illumination, the designed carbonized poplar wood displayed the highest water evaporation efficiency of 86.7%. This is the highest value among other types of carbonized wood, as shown in **Fig. 7d**. This is attributed to the different hemicellulose composition, cellulose, and lignin in the wood leading to different physical properties after the carbonization process [96]. More importantly, this leads to the lower thermal conductivity, high porosity of poplar wood, resulting in excellent heat confinement and outstanding light absorption characteristics. This research reveals the importance of low thermal conductivity of the biomass substrates in localizing heat and preventing underwater heat loss for solar steam generation. The reports on carbonized wood display major drawbacks such as low water evaporation efficiency rose from the non-lateral organization of the wood structure, as well as poor mechanical strength. Besides, cutting trees and utilizing the wood is non-environmentally friendly.

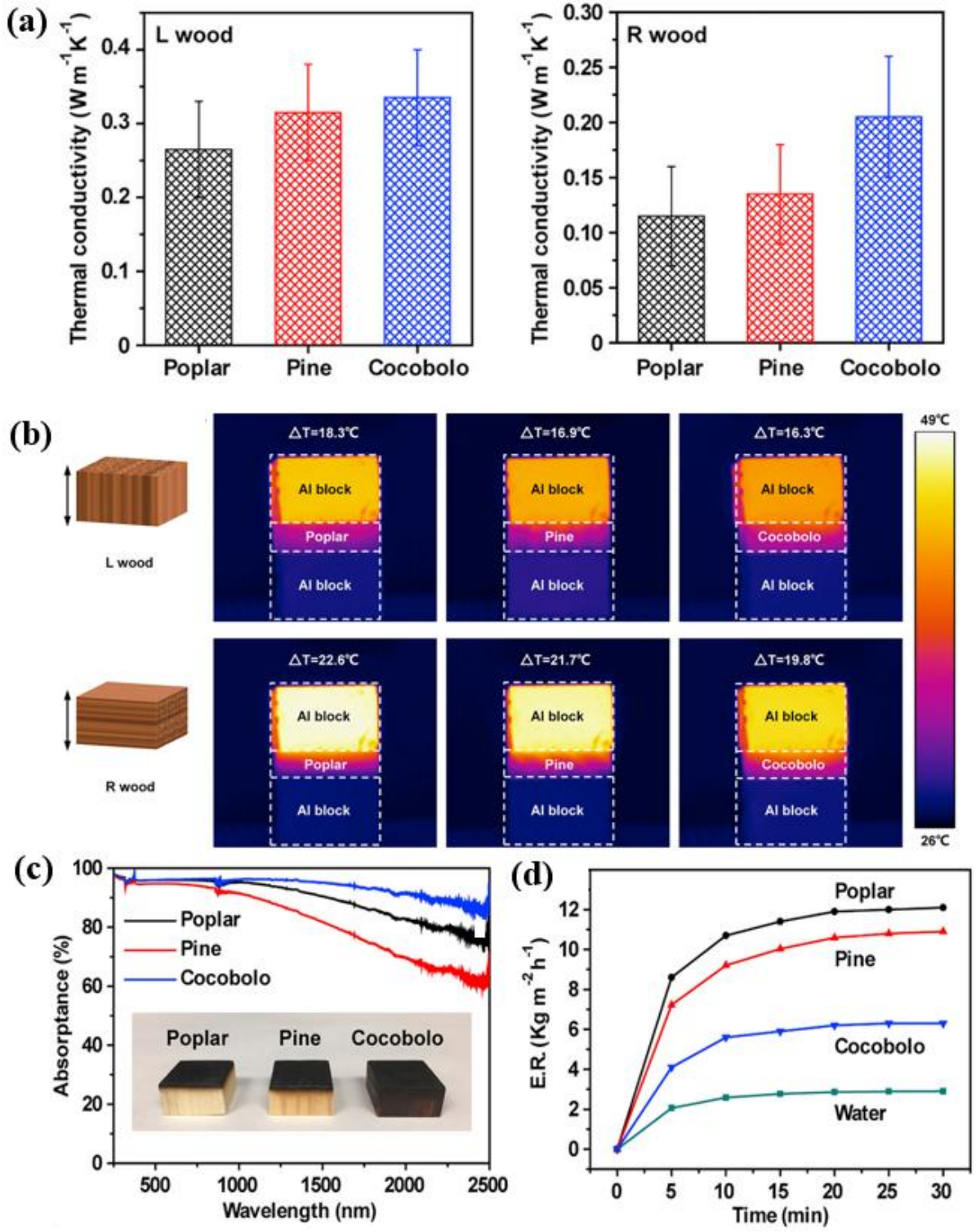

Fig. 7. Comparison of (a) Thermal conductivity characterization of different L woods and R woods of Natural Poplar, Pine, and Cocobolo Wood. (b) IR images of thermal distribution in different L woods and R woods, (c) UV-vis-NIR absorption characteristics. (d) Water evaporation rate under 10 kW/m^2 illumination [95].

The drawbacks of carbonized wood shifted research directions to explore other types of biomass substrates with the aim of solving the shortcoming issues of wood. Diverse materials were investigated as excellent solar steam evaporators such as rice straw, mushroom [76], daikon [62], sunflowers heads [73], lotus [97], and bamboo. Taking carbonized bamboo as an example, it possesses mechanical strength, rapid water transport, and effective heat confinement properties [38]. In 2019, Bian et al. utilized a 3D carbonized bamboo cup (3D CBC) design as a unique water evaporator system [92]. The fabrication process is shown in **Fig. 8a**. 3D CBC exhibited a light absorption of 99.6% (UV-Vis-NIR), which is relatively higher than that of 2D structured carbonized bamboo (94.8%). For SSG performance, a device composed of 3D carbonized bamboo (solar absorber), with PS foam as a thermal insulator wrapped with an air-laid paper as wicking material was designed and used (see **Fig. 8b**). This results in an exceptional water evaporation rate of 3.13 kg m^{-2} h^{-1} under 1 sun illumination. The performance was higher than 2D planar carbonized bamboo, as revealed in **Fig. 8c and d**. The reason of this fascinating performance is attributed to the designed 3D cup structure leading to two main features; (1) heat localization, i.e., reabsorbing the diffuse reflected light and heat and recovering it through the cup walls, and (2) continuous water supply through the inner channels via the capillary force derived from the hydrophilic bamboo fiber. Long et al. demonstrated the use of ethanol-treated carbonized carrot and displayed exceptional water evaporation rate (2.04 kg m^{-2} h^{-1}) and efficiency (127.8%), which exceed the theoretical values [98]. To reveal this, they visualize the heat distribution on the system using IR camera. After the solar intensity of 1 sun, they found that the temperature rapidly reaches 39.5 ^{o}C within 30 s and 48.7 ^{o}C within 3600 s. The underwater temperature was measured, and there was a negligible increase. The excellent performance can be explained by three main points: (i) surface temperature increase across the uneven surface and excellent light-to-heat conversion efficiency; (ii) internal microstructure provides fast water transport characteristics; (iii)

enclosed environment of the experiment resulted in a temperature difference of ~7 ^{o}C between the condenser and the external environment leading to heat exchange and an increase in the evaporation rate. In a recent study, Yu et al reported a highly efficient lotus inspired biomimetic evaporator [97]. The BPTM was fabricated through carbonization, coating with PDA, then with hydrophobic layer at the top to form Janus structure. It incorporated lotus root-like mesopores into bimodal pores containing 3D truss-like macropores. This unique structure resulted in low density, making it self-floating and also leads to lower thermal conductivity (wet state: 0.12 W m^{-1} K^{-1}), substantial water transport, and enhancing the mechanical strength. As a consequence, water evaporation rate of 1.62 kg m^{-2} h^{-1} and efficiency of 74.2% were obtained (1 sun irradiation).

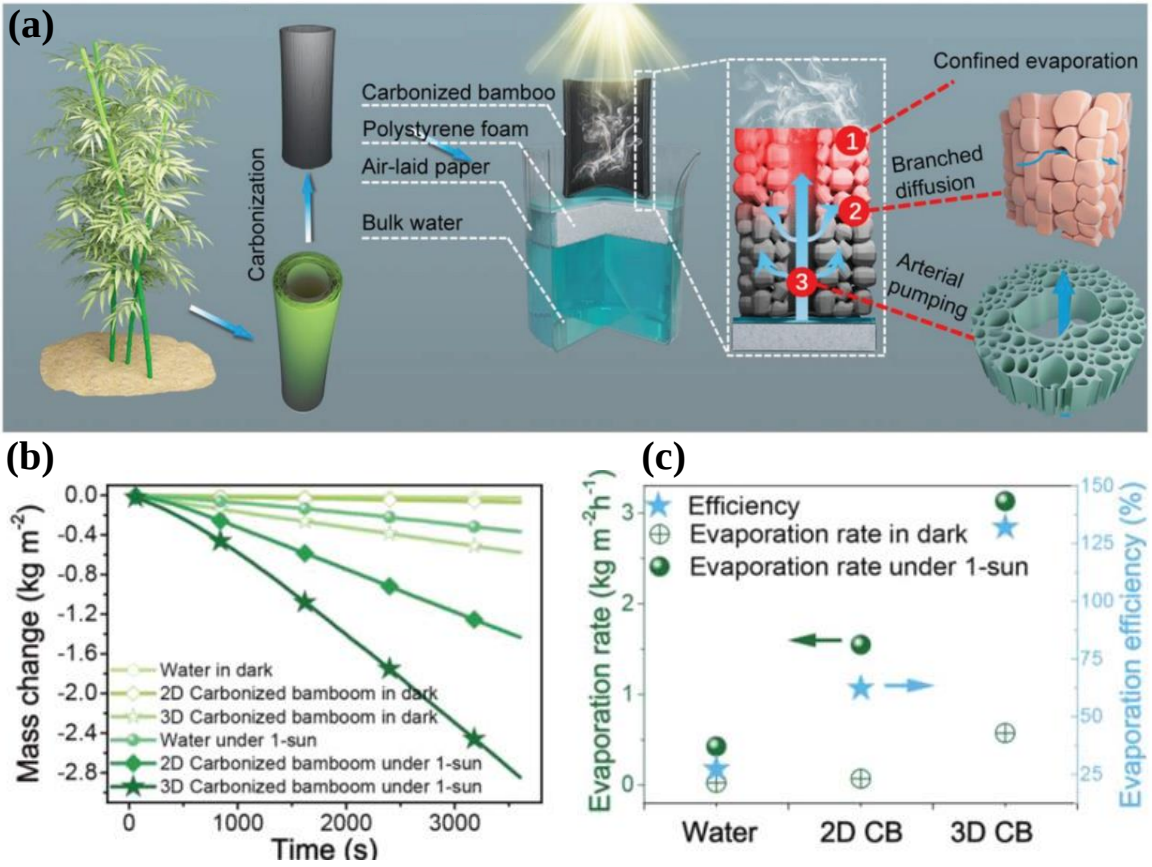

Fig. 8. (a) From the left: bamboo biomass plant, the carbonization process, solar evaporator system compositions, and heat localization mechanism. (b) and (c) Comparison of the evaporation rate of 2D and 3D carbonized bamboo, and the corresponding efficiency under 1 sun irradiation [92].

3.2 Biomass-integrated nanocomposite PTMs

The integration of biomass materials with nanocomposite PTMs were also reported as highly efficient solar steam generation devices. Various PTMs including; carbon materials, plasmonic metals, nanostructure semiconductors, and conjugated polymers, were incorporated with various biomass substrates. In particular, the functionalization of biomass with nanocomposite PTMs is considered a low-cost, easier fabrication process and helps maintain the biomass substrate's physical and chemical properties. This avoids structure collapse and provides long-term structural stability.

3.2.1 Carbon materials-based biomass nanocomposites

Carbon-based materials such as graphene and carbon nanotube (CNT), *etc*. are auxiliary PTMs for SSG. This is attributed to the abundance of π-conjugated bonds enable excellent absorption of solar-light within the whole solar spectrum [63]. In 2017, Hu and co-workers designed a flexible, bendable, and twistable CNT-coated wood PTM fabricated by cutting wood with an electric saw to generate a rough hair-like surface consisting of numerous flower-like micro sheets. The flexibility was obtained by partial removal of hemicellulose and lignin by chemical treatment, followed by the CNT coating process. The CNT layer served as the solar absorber, while the wood acted as the support layer. This lea to outstanding light absorption of 98% at a wavelength of 3000-1200 nm. Under solar irradiation of 10 suns, high water evaporation efficiency of 81% was revealed. Graphene oxide (GO) is a graphene derivative that exhibits excellent water dispersibility, hydrophilicity and rich in functional groups such as carboxyl and hydroxyl groups [20]. This unique property can lead to the facile coating process of GO on biomass-based materials where firm binding of rich carboxyl and hydroxyl groups is formed by hydrogen bonding. Liu et al. demonstrated a bilayered structure consisting of GO-wood composite and revealed a photothermal conversion efficiency of up to 73% under 1 sun

illumination [99]. The high cost and weak wettability hindered the applications of many carbon nanomaterials. To solve this issue, researchers came up with a novel idea of using new generations of cellulose aerogel substrate that attracted tremendous attention as low-cost, scalable, and abundant resources [71]. It can be combined with low concentrations of PTMs and applied as an efficient solar steam generator. Xu's group achieved this through combining RGO with cellulose rice straw and sodium alginate to form a lightweight and flexible 3D porous RGO-BPTM based aerogel [100]. The as-designed materials were capable of absorbing 97% of light across the solar spectrum. Besides, significant heat was controlled from transmitting and thus exhibited excellent heat localization. For SSG experiments, they use an oil-lamp-like setup and examined different sizes of aerogel of 1 cm, 2 cm, and 3 cm. They reveal that 3 cm 3D RGO aerogel displayed the highest solar water evaporation rate of 2.25 kg m^{-2} h^{-1} with high water evaporation efficiency of 89.9% under 1 sun solar irradiation. This is attributed to the low temperature of the top and side of the aerogel which results in low convection and radiation heat loss. Also, the energy gain from outer surrounding enhances the evaporation performance. Wilson et al. reported a candle soot-coated cotton cloth as solar steam generators [40]. The device was prepared by wrapping PS foam with a cotton cloth followed by coating the top portion with candle soot, and then dried at room temperature. After 1 sun illumination, the high solar conversion efficiency of ~80% was achieved. Despite the advantages of low-cost candle soot, the process of burning the candle is not environmentally-friendly for large scales as it can emit greenhouse gases. Upcoming studies should focus on exploration of waste carbonized biomass that could be a viable option for forming an effective biomass based composite PTM.

3.2.2 Conjugated polymer-based biomass nanocomposites

Among the reported PTMs for SSG, a conjugated polymer such as polydopamine (PDA), and polypyrrole (PPy) has been widely investigated and displays incredible performance for solar steam generation. This is attributed to its more straightforward fabrication process, and excellent light absorption caused by strong π-electron localization [8, 101-105]. Additionally, the materials exhibit strong bonding and high stability when attached to various substrates. Zhang et al. reported biomass sponge functionalized PPy as a promising solar steam generator [106]. In brief, they utilized pomelo peel and functionalized it with PPy through oxidative polymerization, followed by freeze-drying. They indicated that after the freeze-drying process, it provided abundant microporous structure that is beneficial for rapid capillary water action. However, after introducing PPy, the pore size has been noticeably increased due to the collapse of some hollow structure within the sponge. The as-designed device displays the capability to adsorb 3 uL of water within 5 s, compared to the device before introducing PPy (within 10 s). This phenomenon is related to the interaction between the N-H bond and Fe^{3+} that are contained in PPy. Under 1 sun illumination, a water evaporation rate of 1.22 kg m^{-2} h^{-1} was obtained. In the research work conducted by Xiao et al., PPy was loaded on sugarcane and applied in SSG [107]. The closely packed open channels and hydrophilicity in the sugarcane substrate facilitate continuous and fast water transport to the solar absorber part, while the attached PPy works as a solar absorber. These features result in a water evaporation rate of 1.59 kg m^{-2} h^{-1} with an efficiency of 90.6%, at 1 sun illumination. Xu and co-workers prepared a PDA-coated pinewood through the self-polymerization process at room temperature [108]. The functionalization of wood morphology and pore channel size remains unchanged. This results in maintaining the mechanical and physical properties of biomass greatly assisting in enhancing the water transport channels. The superhydrophilicity of wood-PDA, due to the abundance of hydroxyl groups (-OH) from PDA, resulted in continuous and fast water transport. PDA acts

639 as an excellent solar absorber for sunlight absorption. As a result, a water evaporation rate of
640 1.38 kg m^{-2} h^{-1}, corresponding to photothermal conversion efficiency of 87% under 1 sun
641 illumination was obtained. Other composite PTM made from conjugated polymers and
642 biomass-based materials (PPy-wood) exhibited a stable water evaporation rate of 1.0 kg m^{-2} h^{-1}
643 and a water evaporation efficiency of >70%, respectively. Besides, a long-term stability test
644 was conducted after storage for up to 45 days, indicating its excellent stability and durability
645 [43].
646 3.2.3 Noble metals-based biomass nanocomposites
647 Noble metals, including Au, Ag, Pd have been investigated as an excellent solar thermal
648 converter for SSG due to their localized surface plasmon resonance (LSPR) effect [109]. For
649 example, Sheng et al. designed ring shapes natural bamboo (thickness of ~1 cm) and deposited
650 Au NPs uniformly on the vessels of the bamboo (**Fig. 9a**) [38]. Bamboo consists of vertically
651 oriented vessel microchannels that provide water capillary force resulting in excellent water
652 transport. It exhibited high absorption efficiency of 99% over the UV-vis-NIR due to the strong
653 LSPR and the internal reflection and trapping through the microchannels. The plasmonic
654 bamboo maintains low thermal conductivity at wet state with a slight increase from 0.30 W m^{-1}
655 k^{-1} (for bamboo) to 0.35 W m^{-1} k^{-1}, thus providing excellent insulating properties. SSG
656 efficiency of 87% was obtained under 10 suns irradiation. Furthermore, they investigated the
657 thickness of the plasmonic bamboo and found that at a low thickness of 1.5 mm, the energy at
658 the absorber part can easily transmit to the bulk water. Besides, a high thickness of 25 mm
659 results in less water evaporation rate due to the hard water absorption. The optimum thickness
660 of 10 mm displays the best performance. Excellent cycling stability was achieved with a stable
661 cycling performance up to 140 hours under 5 sun illumination. In a recent study, Chen et al.
662 also demonstrated a novel hydrophilic 3D solar steam evaporator consisting of plasmonic
663 wooden flower coated with core-shell structured NPs of Ag and PDA (**Fig. 9c**) [110]. The as-

designed 3D evaporators have unique features of: (i) enabling light absorption of 99.9% along the UV-vis-NIR regions (equal to the theoretical black body); (ii) formation of water layers on both sides of the hydrophilic flower petal; (iii) pinholes in the wood leads to suppressing the convection heat loss, and; (iv) significant recovery and utilization of the heat loss. **Fig. 9d** illustrates the working mechanism of a 3D plasmonic wooden flower. This novel plasmonic structure achieved a high-water evaporation rate of 2.08 kg m^{-2} h^{-1} and efficiency up to 97% at 1 sun illumination.

3.2.4 Nanostructured semiconductor materials-based biomass nanocomposites

Nanostructure semiconductor materials are another class of widely studied PTMs in SSG. Its advantages include the simple fabrication process and exhibiting strong light absorption in the broadband solar spectrum. In a semiconductor-based PTMs, when the energy of incident light is higher than that of the semiconductor's bandgap, the light is absorbed, and the electron-hole pairs are generated. Then by the non-radiative relaxation process, photon energy is converted into heat energy [111-113]. To exploit such advantageous features of semiconductor based PTMs, numerous reports demonstrated the incorporation of nano/microstructured of semiconductor PTMs into porous supports such as mixed cellulose acetate membrane (MCE), polytetrafluoroethylene membrane (PTFE), as well as nanocomposite polyvinylidene difluoride (PVDF) membranes. However, the above-mentioned methods exhibited few drawbacks, such as requiring external thermal insulators to reduce the heat losses and needing wick materials for water transport. Recently, biomass-based substrates such as wood demonstrated promising substrate for loading semiconductor-based PTMs to overcome the above-mentioned issues by providing thermal insulation and efficient water transport. For instance, Liu et al. decorated the wood substrate with ~5 nm $CuFeSe_2$ NPs as an effective PTM for a highly efficient solar steam generation [74]. The high light absorption of 99% across the UV-vis-NIR region was obtained, enabling water evaporation efficiency up to 67.7% and

86.2% under 1 and 5 sun illumination, respectively. The high efficiency is attributed to the small size of the NPs enabling effective light absorption and the wood providing microchannels for efficient water transport and allowing heat localization for continuous water evaporation (**Fig. 9d**). Also, the system maintains a stable evaporation rate for a period of 25 cycles (1 h/cycle) at simulated 5 sun illumination. Li et al. described the oxygen-deficient WO_x nanorods modified wood as an effective PTM. The as-designed BPTMs exhibited light absorption of 94% in the UV-vis-NIR region. At 1 solar sun irradiation, water evaporation efficiency of 84% was achieved. Also, cycle stability and reusability test were conducted by drying the wet wood and reusing it, and stable performance was maintained for more than 60 cycles (1h /cycle). In summary, further research effort is required to integrate plasmonic PTMs into other biomass-based substrates.

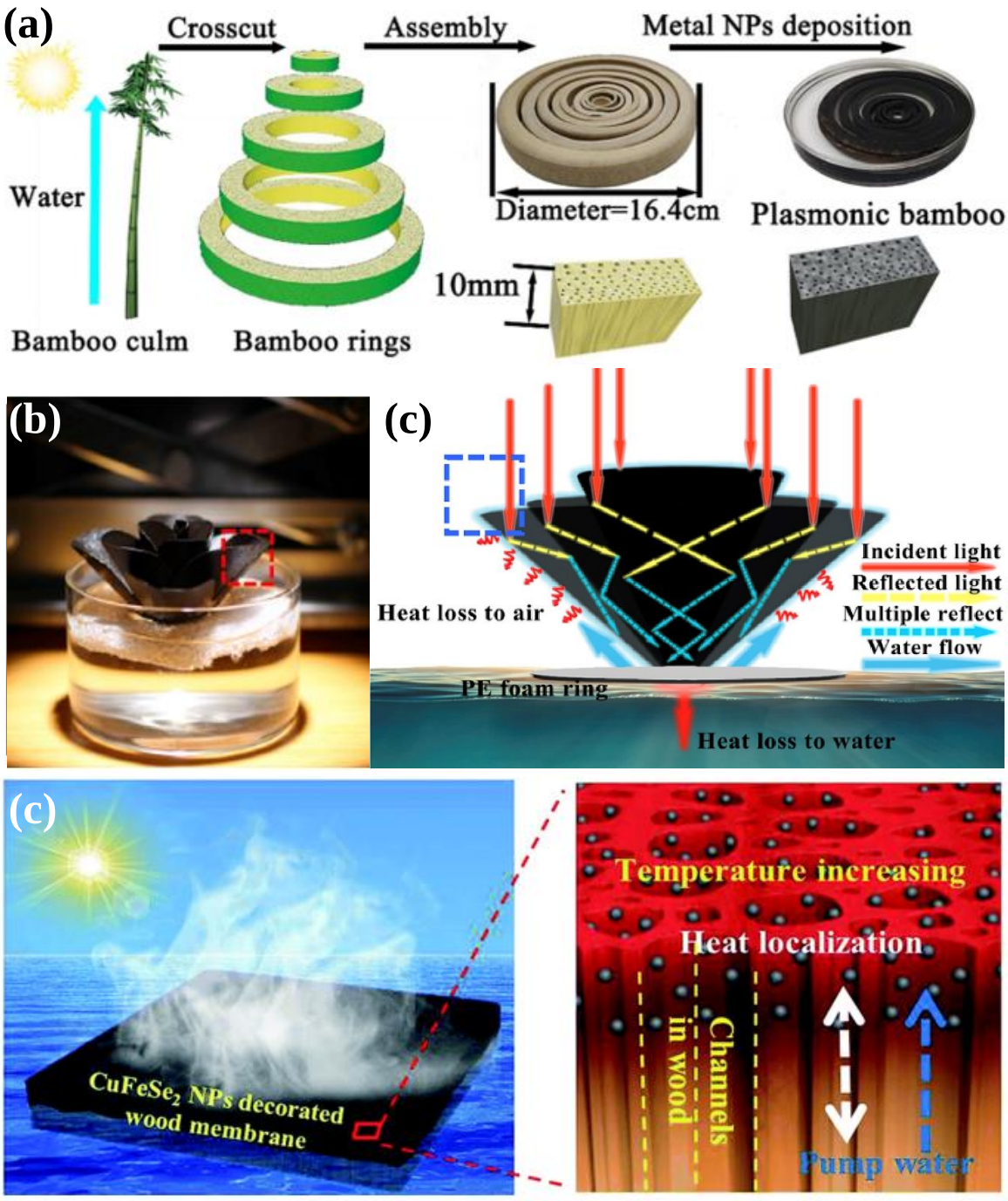

Fig. 9. (a) Schematic illustration of designing bamboo rings and depositions process of plasmonic NPs [38]. (b) Digital image of a plasmonic wooden flower device [110]. (c) Schematic illustration of the working mechanism of the plasmonic wooden flower [110]. (d) $CuFeSe_2$ NPs loaded on a piece of wood, and magnified image shows the mesostructure of the black wood with many channels that localize the heat and facilitate the water transport [74].

3.2.5 Inorganic materials-based biomass nanocomposites

The enhancement in solar steam generation performance by other approaches such as inorganic complexes and Lewis acid catalysts opens opportunity to discover other low-cost, large scale, and more straightforward synthesis approaches. For instance, Li's group employed a low-cost and scalable versatile tannic acid and Fe^{3+} coating on a range of wood substrates with different shapes for solar steam generation device (**Fig. 10a**). The optical properties of such BPTMs were measured, and broadband light absorption of ~ 98% was demonstrated, while their contact angle measurement displayed superhydrophilicity properties (0^o). The water evaporation experiment was carried out on both the 3D wood substrate and the planar wood substrate. Interestingly, at 1 sun irradiation, a water evaporation rate of 1.85 kg m^{-2} h^{-1} was achieved for 3D wood substrate compared to the planar wood substrate (1.34 kg m^{-2} h^{-1}). This work demonstrated the importance of structural design in biomass-based substrates to enhance water evaporation rate by confining the heat, expanding the light absorption area, and the water evaporation area. Chen et al. demonstrated the use of porous, Lewis acid catalyst of aluminophosphate (ALP) to accelerate the formation of a black photothermal carbon layer on the wood substrate (**Fig. 10b**) [114]. The as-prepared BPTM displayed 98% light absorption covering the entire solar spectrum. Hence, water evaporation rate with an efficiency of 1.423 Kg m^{-2} h^{-1} and 90.8% was obtained under 1 sun irradiation. Yu's group developed a novel hybrid biomass-based hydrogel as a cost-effective ($ 14.9 m^{-2}) and highly efficient solar steam generator [91]. It consists of biomass and konjac glucomannan incorporated with Fe-based metal-organic framework NPs (diameter of ~35 nm) with polyvinyl alcohol. The internal structure of microporous (~ 10 μm) hydrogel and the PVA presence lead to rapid water transport and a high evaporation rate of 3.2 kg m^{-2} h^{-1} under one sun irradiation, corresponding to an efficiency of 90%. As such, simple and mixed approach in synthesizing BPTM is a promising avenue for further exploration in near future.

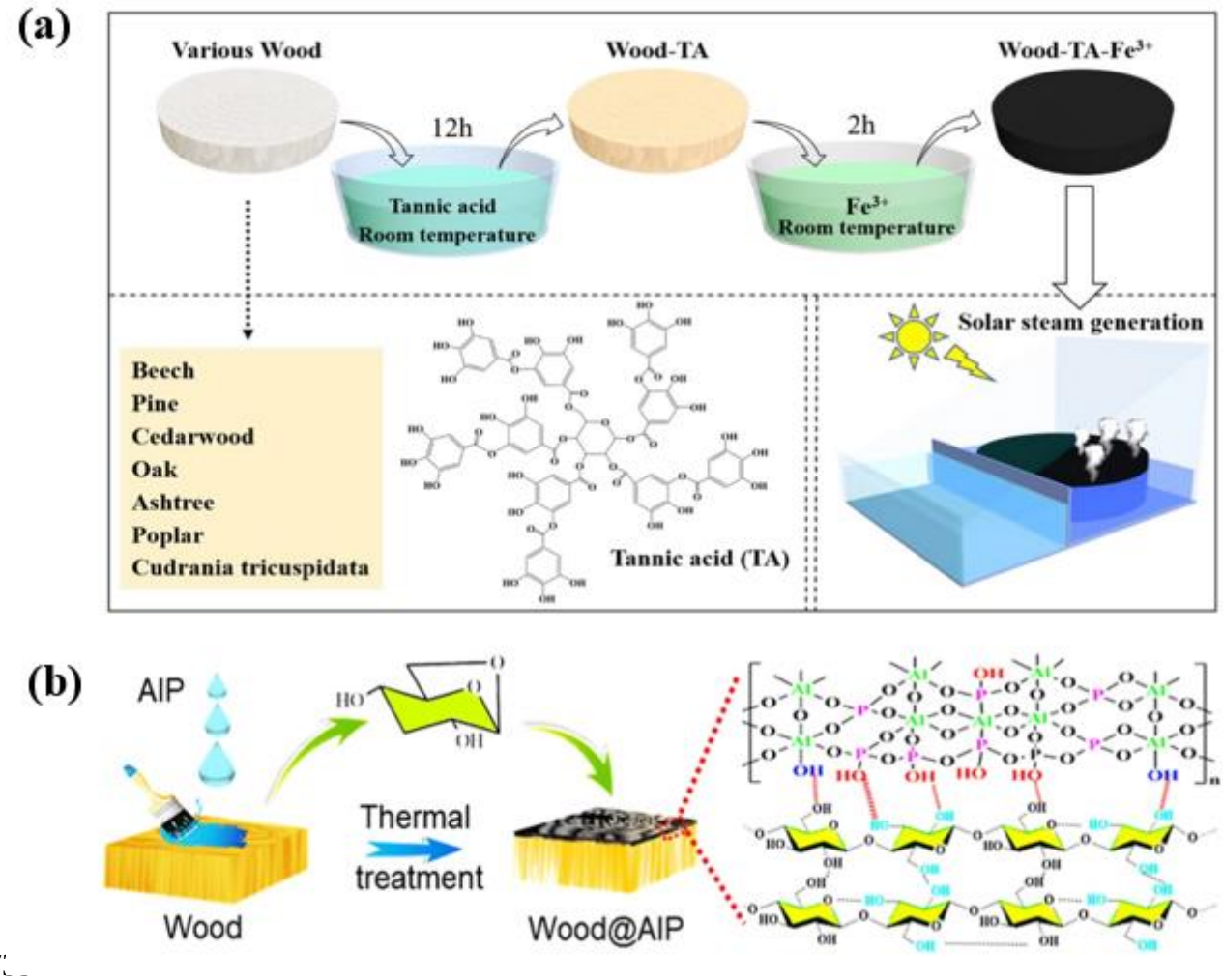

Fig. 10. (a) Schematic illustration of the various processes transforming woods into PTMs incorporated with TA-Fe^{3+} for solar steam generation [45]. (b) Schematic illustration of the possible interaction mechanism between the ALP compound and wood [114].

3.3 Comparison of water evaporation performance of BPTMs

In this section, we discuss the use of various BPTMs for solar steam generation. Two common routes were implemented to achieve biomass PTMs: carbonization of biomass substrate and integration of PTM nanocomposite into biomass substrate. **Fig. 11** reveals the water

evaporation rate and efficiency of biomass based PTMs found in literature. Details of synthesis process, light absorption characteristics and the water evaporation performance are given in **Table S1**. The carbonization process has advantages of excellent solar-to heat and heat-to-vapor generations, which can be achieved directly through utilizing biomass as carbon sources. Unfortunately, most of carbonized biomass possesses weak mechanical strength. Thus, structure collapse and degradation might take place mainly in a harsh environment. However, in the case of bamboo, it has robust mechanical properties compared to many other biomass substrates. For instance, bamboo is four times stronger than wood [60, 92]. Therefore, more attention must be paid to choose biomass with robust mechanical strength to ensure that the carbonization process will not create any structure effect. The integration of PTMs into biomass substrate is another proposed method to overcome the stability issues as this process does not influence the final biomass structure. For example, plasmonic metals display excellent stability and reusability in the harsh environment. However, their relatively high cost and complicated fabrication processes hinder their practical applications. Besides, there are questions about the cost and stability of coated biomass with carbon materials, such as weaker adhesion and detachment of the materials. Biomass based conjugated polymer composite are good candidates for BPTMs. This is attributed to the easy fabrication process, biodegradability, and scalable. Biomass integrated inorganic PTMs such as inorganic complexes or acid-catalyzed are also another promising and versatile strategy towards excellent SSG devices. Despite the promising results, it is still in the early stage and needs further in-depth investigations. The class of PTMs will not influence water evaporation performance. However, the type and the design of the biomass substrate play a significant role, and great attention must be paid into them.

Research on BPTMs revealed that 3D structure biomass (e.g., 3D plasmonic flower, 3D carbonized bamboo cup, and cellulose aerogel, 3D wood-Tannic-Fe^{3+}) display exceptional

769 water evaporation performance exceeding the theoretical values. This could be attributed to
770 three reasons: (1) gaining energy from the environment through heat exchange; (2) large water
771 evaporation area; (3) recovery any heat loss through diffuse reflection and radiation. These
772 features indicate promising potential applications of biomass with a 3D structure for highly
773 efficient SSG systems. We recommend future research focusing on designing and developing
774 3D BPTMs, which are the most impactful tool for SSG. The cost and scalability of PTMs are
775 also essential characteristics for the practical applications that should be taken into account.
776 **Table 4** displays the advantages and disadvantages of various types of BPTMs for SSG
777 applications.
778
779 **Table 4.** Highlights the advantages and the drawbacks of different types of BPTMs

Method	Advantages	Drawback
Carbonized biomass	✓ Direct fabrication process. ✓ Biomass acts as a carbon source. ✓ Excellent water evaporation rate and efficiency, except carbonized wood.	• High synthesis temperature • Poor mechanical strength. • Not environmentally friendly. • Insufficient water evaporation (carbonized wood)
Carbon materials coated on biomass	✓ Good mechanical strength ✓ Reasonable water evaporation rate and efficiency.	• Nanostructured carbon nanomaterials can be expensive. • Coating biomass with carbon materials lower the water transport to evaporator part.
Plasmonic metal based- biomass	✓ Extend the light absorption from UV-Vis to UV-Vis-NIR.	• Plasmonic noble metals are expensive.
Semiconductor based- biomass	✓ Excellent light absorption ✓ Excellent water evaporation rate and efficiency.	• Stability of semiconductor materials when attached to BPTM.

Conjugated polymer based-biomass	✓ Easier fabrication process. ✓ Excellent water evaporation rate and efficiency.	• Photodegradation of conjugated polymers.
Inorganic complexes based-biomass	✓ Low cost. ✓ Easier fabrication process. ✓ High water evaporation rate and efficiency.	• Early stages of development.

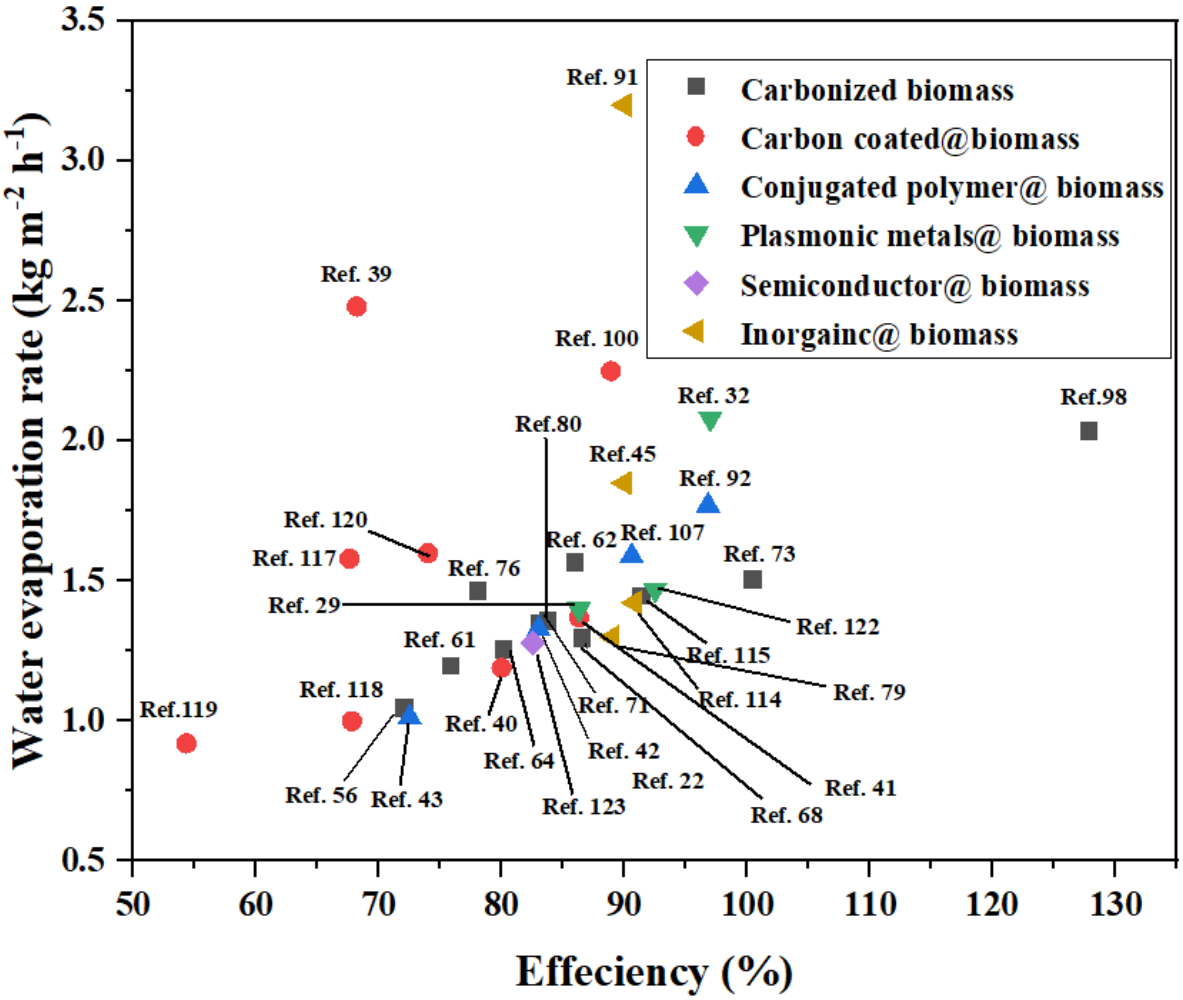

Fig. 11. The reported water evaporation rate and efficiency of BPTMs with the corresponding bibliographic numbers. (■Carbonized biomass [37, 56, 61, 62, 68, 73, 76, 80, 98, 115, 116], ● Carbon coated@biomass [39-41, 100, 117-120], ▲Conjugated polymer@biomass [42-44, 121], ▼ Plasmonic metals@biomass [29, 110, 122], ◆Semiconductor@biomass [123], ◀ Inorganic@biomass [45, 79, 91, 114]).

4. The applications of BPTMs in seawater desalination

Biomass driven solar steam generator holds a great potential as renewable energy driven and green seawater desalination process. Outdoor experiments are essentials to further demonstrate the practical applications. However, there are still challenges in implementing this device to the real-world applications, including the weather conditions which could lower the sunlight intensities leading to the lower condensation rate of distilled water [124].

Various BPTMs were extensively studied using real or simulated seawater. After the desalination process, concentrations of solvated salt ions (Na^+, K^+, Mg^{2+}, and Ca^{2+}) in the collected water is analyzed using an inductively coupled plasma mass spectroscopy (ICP-MS). Besides the clean water production and its water evaporation efficiency, stability, and the anti-fouling properties of the BPTMs is vital for the long term, practical implementation in the field. Most of the reported solar steam generation device performance using natural sunlight. The efficiency was lower than the indoor tests compared with that of simulated sunlight. The main reason is that the natural sunlight received at different places is not precisely equivalent to 1 sun intensity used in the laboratory using a solar simulator.

Li et al. demonstrated seawater desalination via a solar steam generation device using an alkali-treated corn straw (CSA) and microwave treated corn straw (CSMA) coated with polypyrrole PTM. During the process, simulated salt (20% NaCl) was used as a feed solution [44]. Under solar irradiation of 1 sun, the photothermal conversion efficiency of 62.3% and 94.7% were achieved for (CSA) and (CSMA), respectively. The anti-salt crystallization test was conducted under continuous natural sunlight for 30 days, and no salt accumulation on the PTMs was observed. Furthermore, it demonstrates the high rejection of most salt ions (Na^+, K^+, Mg^{2+}, and Ca^{2+}) in saline solution to meet the WHO and EPA standards. Sun et al. designed and fabricated a low-cost, disposable solar steam generation device made of greenhouse glass and disk shape corn stalks coated solar absorber layer of CNT-TiO_2 (**Fig. 12a**). They performed

814 the seawater desalination test using real seawater taken from Bohai, China. As shown in **Fig.**
815 **12b**, the salt concentration (Na^+, Sr^{2+}, Cl^-, and Br^-) after the evaporation was below the WHO
816 and EPA standards. The high salt rejection attributed to the stem marrow of corn stalks,
817 abundant porous basic tissues that act as a salt exchange layer, and providing a self-cleaning
818 surface. Furthermore, an outdoor experiment was conducted in Harbin, China, in April, where
819 the device generated clean water of 4.3-5.8 kg m^{-2} on sunny days and 3.0-3.9 kg m^{-2} on cloudy
820 days [39]. He et al. developed an SSG device consisting of wood-TA-Fe^{3+} PTMs with a 22 cm
821 diameter and 2.8 cm thickness, respectively [45]. Under the natural sunlight, the device
822 exhibited a high clean water production rate of 7.2 kg m^{-2} within 8 hrs of operation, which are
823 enough to satisfy a few people's daily needs for drinking water. Low-cost carbonized daikon
824 (3 US $) has been used as a PTM for seawater desalination via SSG. The device exhibited a
825 salt ion rejection rate ~ 99.9%, meeting the WHO and US EPA standards for drinking water.
826 Additionally, a large-scale device demonstrated that 1 m^2 of carbonized daikon based PTM
827 produced 12 kg of clean water after solar irradiation for 8 hrs. Chen et al. carried out solar
828 desalination performance of delignified wood using real seawater collected from the South
829 China Sea; a schematic illustration of the device is shown in **Fig. 12c**. The seawater
830 desalination test was conducted from 10:00 am to 4:00 pm under natural sunlight (~70 mW
831 cm^{-2}). The water evaporation rate of ~ 0.65 kg m^{-2} h^{-1} was obtained and the salt ions
832 concentration in the collected water was below the standard level of WHO and US EPA (**Fig.**
833 **12d**). **Table S.2** lists other related works on this application. As described above, BPTMs
834 showed a promising result in solar desalination applications. The salt can be cleaned-up via a
835 self-cleaning process; thus, long-term reusability with stable performance can be achieved.

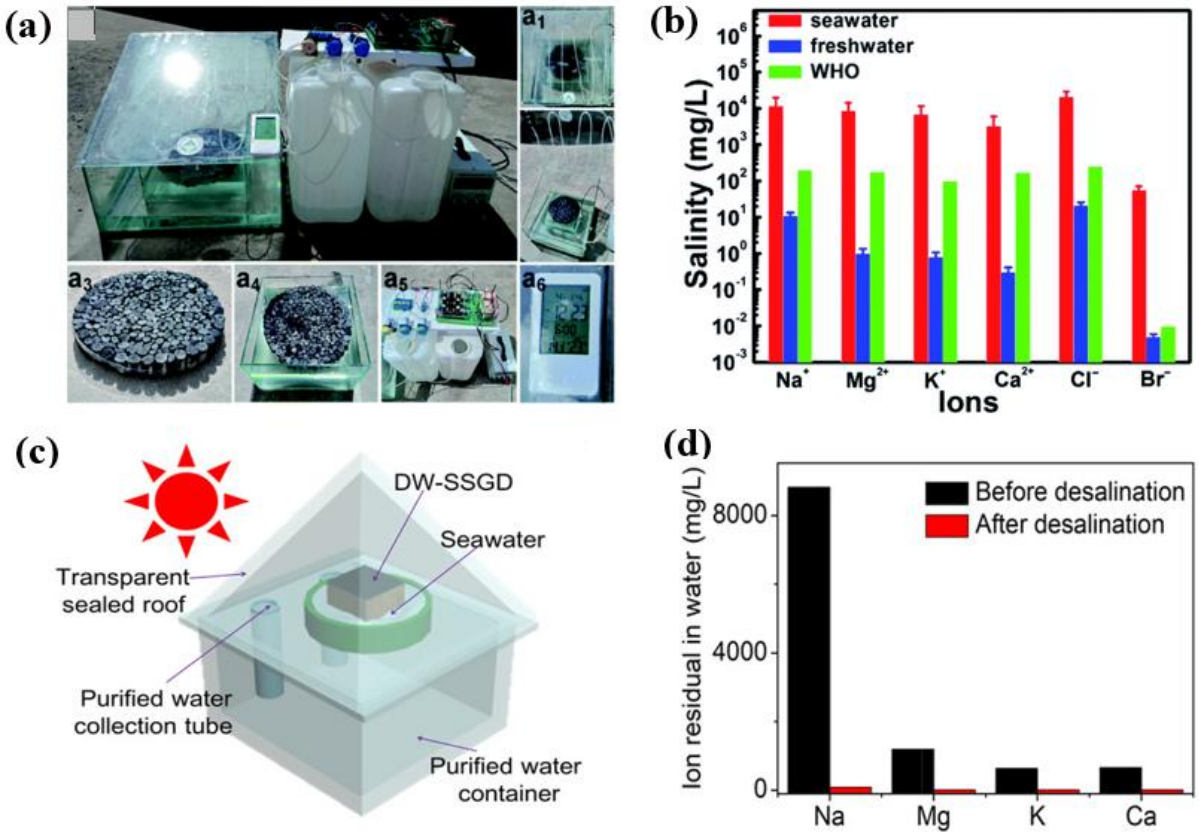

836

837 **Fig. 12.** (a) Photograph of corn stalk derived solar steam generator for water desalination. (b)
838 Changes in the ion concentration in freshwater after the evaporation and seawater before
839 evaporation (taken from Bohai, China) [39]. (c) Schematic illustration of the seawater
840 desalination setup. (d) Measured concentrations of four primary ions in an actual seawater
841 sample before and after the desalination [79].

842

843 5. Durability and stability of BPTMs

844 Long term recyclability with stable performance is an essential factor in designing commercial
845 and practical solar steam generation devices. The harsh feedwater environment accelerates the
846 potential degradation of BPTMs. Therefore, BPTMs with good stability, recyclability, and
847 durability are essential for the long term, large scale implementation of these devices in real-
848 world applications. Numerous studies investigated the stability of BPTMs in various feed water
849 environments, including acidic, neutral, and alkaline conditions [60]. For instance, Zhu et al.
850 demonstrated the stability of plasmonic metal NPs-wood composite PTM by the
851 ultrasonication process of the composite PTM for 30 min in neutral, acidic, and basic

conditions. They found out that metals are well attached, and no leaching of the metal NPs was observed to realize excellent structure stability. Kiriarachchi et al. investigated the stability of plasmonic metal NPs-cotton composite PTM under different pH conditions under the solar irradiation of 5 suns for 30 mins. Water evaporation rate of 6.72, 6.70, and 6.84 kg m^{-2} h^{-1} was achieved at pH 2, 7, and 10, respectively [29]. Similarly, other BPTM nanocomposite (PPy-wood) exhibited a stable water evaporation rate of 1.0 kg m^{-2} h^{-1} and a water evaporation efficiency of >70%, respectively. A long-term stability test was conducted after storage for up to 45 days, indicating its excellent stability and durability [43]. Recently, bamboo attracted the researcher's attention as a robust BPTM because it has excellent mechanical stability, which is four times stronger than wood [92]. Bian et al. examined the long term stability of 3D carbonized bamboo by placing the BPTM under light illumination for 16 hours [92]. After the light irradiation, they noticed the salt crystalized on the outer and inner surface of the carbonized bamboo. With continuous water evaporation, the crystallized salts were dissolved, demonstrating its self-cleaning ability. Furthermore, high water evaporation rate of 3.11 kg m^{-2} h^{-1} was achieved, with stabile evaporation rate performance for 15 cycles (8h illumination/cycle). Chen et al. demonstrated the excellent mechanical strength of delignified wood, which was fabricated with assistance from DES. Resulting from the partial entrance of DES into the cell walls of the wood and forming hydrogen bond, which acts as a glue providing such good mechanical stability [79]. Based on the reported results, many articles demonstrate the excellent stability of various BPTMs at the lab scale. However, there aren’t many studies revealing the stability and the reusability of large scale BPTM based devices under natural sunlight, and humidity should be counted for further implementation of these devices in real applications.

6. Conclusion and opportunities

The application of BPTMs in SSG demonstrated a promising result in diverse water purification applications. This is attributable to their sustainability, naturally abundant and low-cost biomass substrates, which can be integrated with various classes of PTMs. In this review, we illustrated the advantages and the roles of diverse biomass substrates (after incorporating with PTMs) in meeting all the criteria for high-performance SSG. These investigations confirm that compared with various substrates, biomass substrates display exceptional performance for SSG due to the following reasons: (i) presence of high porosity and microchannels resulting in multiple internal light reflection and trapping; (ii) relatively low thermal conductivity, hence localized heat at the air-water interfaces and minimized heat losses; (iii) surface wettability and the rich interconnected microchannels leads to efficient water supply channel, and; (iv) the micro-size channels, biomass compositions and hydrophilicity lead to extraordinary anti-salt crystallization, and self-cleaning properties. Nevertheless, there are still some existing challenges that should be addressed. These include:

1. The re-utilization of biomass and developing them into effective PTM is an attractive strategy that would be more economical and environmentally friendly. Furthermore, other biomass categories, such as animal residues or waste, might be a potential avenue for further research as a potential PTM material for solar steam generation.
2. The investigations of new classes of PTMs integrated with biomass substrate is also worth exploring to improve the solar-thermal conversion efficiency. Therefore, it is crucial to synthesize, discover, and explore low-cost and scalable PTMs with controlled size and morphologies.
3. 3D structure BPTMs prove to achieve remarkable solar water evaporation rate and efficiency. Despite such magnificent achievement, its performance translation to real outdoor, large scale device development is yet to be realized, where several challenges

need to be overcome. Moreover, proper economic analysis and the overall cost of BPTM devices require further exploration. This study is highly desired for the commercialization of these devices in real applications and industry adoption.

4. Particular attention should also be paid to the structure stability and long-term reusability as it is one of the main criteria for practical applications. The stability performance of BPTMs should be investigated using real seawater and under natural sunlight. Also, the effect of temperature together with the humidity is worthy of being explored. Besides, mechanical properties should be considered for the use of biomass substrates. Similarly, more strategies for modifications of biomass substrates to further enhance its mechanical strength is required.
5. The techno-economic and designing of large area BPTMs devices is seldom mentioned. The biomass materials are low cost. However, the cost of carbonizations or the integration of biomass substrates with nanoscale PTMs needs to be considered.

The clean water production using sustainable paths via BPTMs is promising even though challenges still exist. Further research efforts in the developments of BPTMs based SSG devices will undoubtedly contribute to the green, energy-efficient supply of clean water to people, especially in remote regions. This might provide alternative solutions to energy-intensive, non-environmentally friendly processes used in current water desalination.

Author contribution

Idris Ibrahim: Conceptualization, Methodology, Data Curation, Writing - Original Draft, Review and Editing. Vrushank Bhoopal: Writing - Original Draft, Data Curation. Morteza Afsari: Writing - Original Draft. Dong Han Seo: Writing - Review & Editing. Ho Kyong Shon:

928 Supervision, Resources, Writing- Review and Editing. Leonard Tijing: Supervision,
929 Conceptualization, Resources, Writing- Review and Editing.
930
931 **Conflict of interest**
932 Authors hereby confirm that this manuscript has not been published and is not under
933 consideration elsewhere. Authors declare no conflict of interest.
934
935 **Acknowledgments**
936 Idris Ibrahim is grateful for the financial support from the Australian Government through
937 International Research Training Program (IRTP) scholarship for his PhD studies. D.H.S
938 acknowledges the support of UTS Chancellor's Postdoctoral Research Fellowship scheme. L.T
939 appreciates the support from CTWW internal grant. H.K.S expresses gratitude for the support
940 by the Korea Environment Industry & Technology Institute (KEITI) through Industrial
941 Facilities & Infrastructure Research Program, funded by Korea Ministry of Environment
942 (MOE) (1485016424), and also from the Australian Research Council (ARC) support.

References

[1] T. Leiknes, The effect of coupling coagulation and flocculation with membrane filtration in water treatment: A review, J. Environ. Sci., 21 (2009), pp. 8-12.
[2] J. He, Z. Zhang, C. Xiao, F. Liu, H. Sun, Z. Zhu, W. Liang, A. Li, High-performance salt-rejecting and cost-effective superhydrophilic porous monolithic polymer foam for solar steam generation, ACS Appl. Mater. Interfaces, 12 (2020), pp. 16308-16318.
[3] S.A. Kalogirou, Seawater desalination using renewable energy sources, Prog. Energy Combust. Sci., 31 (2005), pp. 242-281.
[4] M.A. Shannon, P.W. Bohn, M. Elimelech, J.G. Georgiadis, B.J. Marinas, A.M. Mayes, Science and technology for water purification in the coming decades, Nature, (2008), pp. 301-310.
[5] Q. Zhao, C. Du, Y. Jia, J. Yuan, G. Song, X. Zhou, S. Sun, C. Zhou, L. Zhao, S. Yang, Solar-powered Janus membrane for one-step conversion of sewage to clean water, Chem. Eng. J., 387 (2020), p. 124131.
[6] X. Wang, M.-L. Hsieh, J. Bur, S.-Y. Lin, S. Narayanan, Capillary-driven solar-thermal water desalination using a porous selective absorber, Mater. Today Energy, 17 (2020), p. 100453.
[7] Y. Wang, X. Wu, B. Shao, X. Yang, G. Owens, H. Xu, Boosting solar steam generation by structure enhanced energy management, Sci. Bull., 65 (2020), pp. 1380-1388.
[8] X. Wu, G.Y. Chen, G. Owens, D. Chu, H. Xu, Photothermal materials: a key platform enabling highly efficient water evaporation driven by solar energy, Mater. Today Energy, 12 (2019), pp. 277-296.
[9] C. Chen, Y. Kuang, L. Hu, Challenges and opportunities for solar evaporation, Joule, 3 (2019), pp. 683-718.
[10] Y. Fu, G. Wang, X. Ming, X. Liu, B. Hou, T. Mei, J. Li, J. Wang, X. Wang, Oxygen plasma treated graphene aerogel as a solar absorber for rapid and efficient solar steam generation, Carbon, 130 (2018), pp. 250-256.
[11] X. Wu, M.E. Robson, J.L. Phelps, J.S. Tan, B. Shao, G. Owens, H. Xu, A flexible photothermal cotton-CuS nanocage-agarose aerogel towards portable solar steam generation, Nano Energy, 56 (2019), p. 708-715.
[12] W. Cai, Z. Li, C. Ma, W. Guo, B. Zou, S. Qiu, L. Song, Z. Gui, Y. Hu, Effect of crystal defects on solar steam generation performance of black phosphorous nanosheets, Mater. Today Energy, 19 (2021), p. 100553.
[13] I. Ibrahim, D.H. Seo, A.M. McDonagh, H.K. Shon, L. Tijing, Semiconductor photothermal materials enabling efficient solar steam generation toward desalination and wastewater treatment, Desalination, (2020), p. 114853.
[14] J. Gong, J. Liang, K. Sumathy, Review on dye-sensitized solar cells (DSSCs): fundamental concepts and novel materials, Renew. Sustain. Energy Rev., 16 (2012), pp. 5848-5860.
[15] C. Xie, F. Yan, Flexible photodetectors based on novel functional materials, Small, 13 (2017), p. 1701822.
[16] A. Kudo, Y. Miseki, Heterogeneous photocatalyst materials for water splitting, Chem. Soc. Rev., 38 (2009), pp. 253-278.
[17] O. Neumann, A.S. Urban, J. Day, S. Lal, P. Nordlander, N.J. Halas, Solar vapor generation enabled by nanoparticles, ACS Nano, 7 (2013), p. 42-49.
[18] H. Ghasemi, G. Ni, A.M. Marconnet, J. Loomis, S. Yerci, N. Miljkovic, G. Chen, Solar steam generation by heat localization, Nat. Commun., 5 (2014), p. 4449.
[19] V. Kashyap, H. Ghasemi, Solar heat localization: concept and emerging applications, J. Mater. Chem. A, 8 (2020), pp. 7035-7065.

[20] X. Hu, W. Xu, L. Zhou, Y. Tan, Y. Wang, S. Zhu, J. Zhu, Tailoring graphene oxide-based aerogels for efficient solar steam generation under one sun, Adv. Mater., 29 (2017), p. 1604031.
[21] G. Ni, G. Li, S.V. Boriskina, H. Li, W. Yang, T. Zhang, G. Chen, Steam generation under one sun enabled by a floating structure with thermal concentration, Nat. Energy, 1 (2016), pp. 1-7.
[22] Y. Li, T. Gao, Z. Yang, C. Chen, Y. Kuang, J. Song, C. Jia, E.M. Hitz, B. Yang, L. Hu, Graphene oxide-based evaporator with one-dimensional water transport enabling high-efficiency solar desalination, Nano Energy, 41 (2017), pp. 201-209.
[23] J. He, Y. Fan, C. Xiao, F. Liu, H. Sun, Z. Zhu, W. Liang, A. Li, Enhanced solar steam generation of hydrogel composite with aligned channel and shape memory behavior, Compos. Sci. Technol., 204 (2021), p. 108633.
[24] L. Chen, M. Xia, J. Du, X. Luo, L. Zhang, A. Li, Superhydrophilic and oleophobic porous architectures based on basalt fibers as oil-repellent photothermal materials for solar steam generation, ChemSusChem, 13 (2020), pp. 493-500.
[25] C. Xiao, W. Liang, L. Chen, J. He, F. Liu, H. Sun, Z. Zhu, A. Li, Janus poly (ionic liquid) monolithic photothermal materials with superior salt-rejection for efficient solar steam generation, ACS Appl. Energy Mater., 2 (2019), pp. 8862-8870.
[26] G. Wang, Y. Fu, A. Guo, T. Mei, J. Wang, J. Li, X. Wang, Reduced graphene oxide–polyurethane nanocomposite foam as a reusable photoreceiver for efficient solar steam generation, Chem. Mater., 29 (2017), pp. 5629-5635.
[27] B. Huo, D. Jiang, X. Cao, H. Liang, Z. Liu, C. Li, J. Liu, N-doped graphene/carbon hybrid aerogels for efficient solar steam generation, Carbon, 142 (2019), pp. 13-19.
[28] G. Cheng, X. Wang, X. Liu, Y. He, B.V. Balakin, Enhanced interfacial solar steam generation with composite reduced graphene oxide membrane, Sol. Energy, 194 (2019), pp. 415-430.
[29] H.D. Kiriarachchi, F.S. Awad, A.A. Hassan, J.A. Bobb, A. Lin, M.S. El-Shall, Plasmonic chemically modified cotton nanocomposite fibers for efficient solar water desalination and wastewater treatment, Nanoscale, 10 (2018), pp. 18531-18539.
[30] W. Huang, P. Su, Y. Cao, C. Li, D. Chen, X. Tian, Y. Su, B. Qiao, J. Tu, X. Wang, Three-dimensional hierarchical CuxS-based evaporator for high-efficiency multifunctional solar distillation, Nano Energy, 69 (2020), p. 104465.
[31] H. Wang, Q. Dong, J. Yao, Z. Shao, J. Ma, X. Chen, Colorless silk/copper sulfide hybrid fiber and fabric with spontaneous heating property under sunlight, Biomacromolecules, 21 (2020), pp. 1596-1603.
[32] Z. Guo, Z. Chen, Z. Shi, J. Qian, J. Li, T. Mei, J. Wang, X. Wang, P. Shen, Stable metallic 1T phase engineering of molybdenum disulfide for enhanced solar vapor generation, Sol. Energy Mater. Sol. Cell., 204 (2020), p. 110227.
[33] Y. Sun, J. Gao, Y. Liu, H. Kang, M. Xie, F. Wu, H. Qiu, Copper sulfide-macroporous polyacrylamide hydrogel for solar steam generation, Chem. Eng. Sci., 207 (2019), pp. 516-526.
[34] X. Wang, Q. Liu, S. Wu, B. Xu, H. Xu, Multilayer polypyrrole nanosheets with self-organized surface structures for flexible and efficient solar–thermal energy conversion, Adv. Mater., 31 (2019), p 1807716.
[35] W. Li, Z. Li, K. Bertelsmann, D.E. Fan, Portable low-pressure solar steaming-collection unisystem with polypyrrole origamis, Adv. Mater., 31 (2019), p. 1900720.
[36] D. Hao, Y. Yang, B. Xu, Z. Cai, Efficient solar water vapor generation enabled by water-absorbing polypyrrole coated cotton fabric with enhanced heat localization, Appl. Therm. Eng., 141 (2018), pp. 406-412.

[37] Y. Lu, X. Wang, D. Fan, H. Yang, H. Xu, H. Min, X. Yang, Biomass derived Janus solar evaporator for synergic water evaporation and purification, Sustain. Mater. Technol., 25 (2020), p. e00180.
[38] C. Sheng, N. Yang, Y. Yan, X. Shen, C. Jin, Z. Wang, Q. Sun, Bamboo decorated with plasmonic nanoparticles for efficient solar steam generation, Appl. Therm. Eng., 167 (2020), p. 114712.
[39] Z. Sun, W. Li, W. Song, L. Zhang, Z. Wang, A high-efficiency solar desalination evaporator composite of corn stalk, Mcnts and TiO_2: ultra-fast capillary water moisture transportation and porous bio-tissue multi-layer filtration, J. Mater. Chem. A, 8 (2020), pp. 349-357.
[40] H.M. Wilson, S.R. AR, A.E. Parab, N. Jha, Ultra-low cost cotton based solar evaporation device for seawater desalination and waste water purification to produce drinkable water, Desalination, 456 (2019), pp. 85-96.
[41] S. Gao, X. Dong, J. Huang, J. Dong, F.D. Maggio, S. Wang, F. Guo, T. Zhu, Z. Chen, Y. Lai, Bioinspired soot-deposited Janus fabrics for sustainable solar steam generation with salt-rejection, Glob. Chall., 3 (2019), p. 1800117.
[42] W. Huang, G. Hu, C. Tian, X. Wang, J. Tu, Y. Cao, K. Zhang, Nature-inspired salt resistant polypyrrole–wood for highly efficient solar steam generation, Sustain. Energy Fuels, 3 (2019), pp. 3000-3008.
[43] Z. Wang, Y. Yan, X. Shen, C. Jin, Q. Sun, H. Li, A wood–polypyrrole composite as a photothermal conversion device for solar evaporation enhancement, J. Mater. Chem. A, 7 (2019), pp. 20706-20712.
[44] J. Li, X. Zhou, P. Mu, F. Wang, H. Sun, Z. Zhu, J. Zhang, W. Li, A. Li, Ultralight biomass porous foam with aligned hierarchical channels as salt-resistant solar steam generators, ACS Appl. Mater. Interfaces, 12 (2019), pp. 798-806.
[45] F. He, M. Han, J. Zhang, Z. Wang, X. Wu, Y. Zhou, L. Jiang, S. Peng, Y. Li, A simple, mild and versatile method for preparation of photothermal woods toward highly efficient solar steam generation, Nano Energy, 71 (2020), p. 104650.
[46] Y. Lin, H. Xu, X. Shan, Y. Di, A. Zhao, Y. Hu, Z. Gan, Solar steam generation based on the photothermal effect: from designs to applications, and beyond, J. Mater. Chem. A, 7 (2019), pp. 19203-19227.
[47] H. Li, Z. Yan, Y. Li, W. Hong, Latest development in salt removal from solar-driven interfacial saline water evaporator: Advanced designs and challenges, Water Res., (2020), p. 115770.
[48] V.D. Dao, H.S. Choi, Carbon-based sunlight absorbers in solar-driven steam generation devices, Glob. Chall., 2 (2018), p. 1700094.
[49] T. Yang, H. Lin, K.-T. Lin, B. Jia, Carbon-based absorbers for solar evaporation: Steam generation and beyond, Sustain. Mater. Technol., (2020), p. e00182.
[50] X. Li, B. Zhu, J. Zhu, Graphene oxide based materials for desalination, Carbon, 146 (2019) 320-328.
[51] J. Liang, H. Liu, J. Yu, L. Zhou, J. Zhu, Plasmon-enhanced solar vapor generation, Nanophotonics, 8 (2019), pp. 771-786.
[52] J. Zhou, Y. Gu, P. Liu, P. Wang, L. Miao, J. Liu, A. Wei, X. Mu, J. Li, J. Zhu, Development and evolution of the system structure for highly efficient solar steam generation from zero to three dimensions, Adv. Funct. Mater., 29 (2019), p. 1903255.
[53] F. Liu, W. Liang, C. Wang, C. Xiao, J. He, G. Zhao, Z. Zhu, H. Sun, A. Li, Superhydrophilic and mechanically robust phenolic resin as double layered photothermal materials for efficient solar steam generation, Mater. Today Energy, 16 (2020), p. 100375.
[54] V.-D. Dao, N.H. Vu, S. Yun, Recent advances and challenges for solar-driven water evaporation system toward applications, Nano Energy, 68 (2020), p. 104324.

[55] L. Shi, X. Wang, Y. Hu, Y. He, Y. Yan, Solar-thermal conversion and steam generation: a review, Appl. Therm. Eng., 179 (2020), p. 115691.
[56] G. Xue, K. Liu, Q. Chen, P. Yang, J. Li, T. Ding, J. Duan, B. Qi, J. Zhou, Robust and low-cost flame-treated wood for high-performance solar steam generation, ACS Appl. Mater. Interfaces, 9 (2017), pp. 15052-15057.
[57] L. Zhou, S. Zhuang, C. He, Y. Tan, Z. Wang, J. Zhu, Self-assembled spectrum selective plasmonic absorbers with tunable bandwidth for solar energy conversion, Nano Energy, 32 (2017), pp. 195-200.
[58] T. Wu, H. Li, M. Xie, S. Shen, W. Wang, M. Zhao, X. Mo, Y. Xia, Incorporation of gold nanocages into electrospun nanofibers for efficient water evaporation through photothermal heating, Mater. Today Energy, 12 (2019), pp. 129-135.
[59] T. Li, Q. Fang, H. Lin, F. Liu, Enhancing solar steam generation through manipulating the heterostructure of PVDF membranes with reduced reflection and conduction, J. Mater. Chem. A, 7 (2019), pp. 17505-17515.
[60] M. Zhu, Y. Li, F. Chen, X. Zhu, J. Dai, Y. Li, Z. Yang, X. Yan, J. Song, Y. Wang, Plasmonic wood for high-efficiency solar steam generation, Adv. Energy Mater., 8 (2018), p. 1701028.
[61] Q. Fang, T. Li, Z. Chen, H. Lin, P. Wang, F. Liu, Full biomass-derived solar stills for robust and stable evaporation to collect clean water from various water-bearing media, ACS Appl. Mater. Interfaces, 11 (2019), pp.10672-10679.
[62] M. Zhu, J. Yu, C. Ma, C. Zhang, D. Wu, H. Zhu, Carbonized daikon for high efficient solar steam generation, Sol. Energy Mater. Sol. Cell., 191 (2019), pp. 83-90.
[63] C. Zhang, H.Q. Liang, Z.K. Xu, Z. Wang, Harnessing solar-driven photothermal effect toward the water–energy nexus, Adv. Sci., 6 (2019), p. 1900883.
[64] P. Qiu, F. Liu, C. Xu, H. Chen, F. Jiang, Y. Li, Z. Guo, Porous three-dimensional carbon foams with interconnected microchannels for high-efficiency solar-to-vapor conversion and desalination, J. Mater. Chem. A, 7 (2019), pp. 13036-13042.
[65] M. Gao, L. Zhu, C.K. Peh, G.W. Ho, Solar absorber material and system designs for photothermal water vaporization towards clean water and energy production, Energy Environ. Sci., 12 (2019), pp. 841-864.
[66] J. Lee, K. Kim, S.H. Park, G.Y. Yoon, J. Kim, S.J. Lee, Macroporous photothermal bilayer evaporator for highly efficient and self-cleaning solar desalination, Nano Energy, 77 (2020), p. 105130.
[67] X. Wu, Z. Wu, Y. Wang, T. Gao, Q. Li, H. Xu, All-Cold Evaporation under one sun with zero energy loss by Using a Heatsink Inspired Solar Evaporator, Adv. Sci., (2021), p. 2002501.
[68] J. Fang, J. Liu, J. Gu, Q. Liu, W. Zhang, H. Su, D. Zhang, Hierarchical porous carbonized lotus seedpods for highly efficient solar steam generation, Chem. Mater., 30 (2018), pp. 6217-6221.
[69] J. Liu, Q. Liu, D. Ma, Y. Yuan, J. Yao, W. Zhang, H. Su, Y. Su, J. Gu, D. Zhang, Simultaneously achieving thermal insulation and rapid water transport in sugarcane stems for efficient solar steam generation, J. Mater. Chem. A, 7 (2019), pp. 9034-9039.
[70] H. Liu, C. Chen, G. Chen, Y. Kuang, X. Zhao, J. Song, C. Jia, X. Xu, E. Hitz, H. Xie, High-performance solar steam device with layered channels: artificial tree with a reversed design, Adv. Energy Mater., 8 (2018), p. 1701616.
[71] Q. Zhang, L. Li, B. Jiang, H. Zhang, N. He, S. Yang, D. Tang, Y. Song, Flexible and mildew-resistant wood-derived aerogel for stable and efficient solar desalination, ACS Appl. Mater. Interfaces, 12 (2020), pp. 28179-28187.
[72] H. Song, Y. Liu, Z. Liu, M.H. Singer, C. Li, A.R. Cheney, D. Ji, L. Zhou, N. Zhang, X. Zeng, Cold vapor generation beyond the input solar energy limit, Adv. Sci., 5 (2018), p. 1800222.

[73] P. Sun, W. Zhang, I. Zada, Y. Zhang, J. Gu, Q. Liu, H. Su, D. Pantelic, B. Jelenkovic, D. Zhang, 3D-structured carbonized sunflower heads for improved energy efficiency in solar steam generation, ACS Appl. Mater. Interfaces, 12 (2019), pp. 2171-2179.
[74] H. Liu, C. Chen, H. Wen, R. Guo, N.A. Williams, B. Wang, F. Chen, L. Hu, Narrow bandgap semiconductor decorated wood membrane for high-efficiency solar-assisted water purification, J. Mater. Chem. A, 6 (2018), pp.18839-18846.
[75] H. Zhang, L. Li, B. Jiang, Q. Zhang, J. Ma, D. Tang, Y. Song, Highly thermally insulated and superhydrophilic corn straw for efficient solar vapor generation, ACS Appl. Mater. Interfaces, 12 (2020), pp. 16503-16511.
[76] N. Xu, X. Hu, W. Xu, X. Li, L. Zhou, S. Zhu, J. Zhu, Mushrooms as efficient solar steam-generation devices, Adv. Mater., 29 (2017), p. 1606762.
[77] B. Shao, Y. Wang, X. Wu, Y. Lu, X. Yang, G.Y. Chen, G. Owens, H. Xu, Stackable nickel–cobalt@ polydopamine nanosheet based photothermal sponges for highly efficient solar steam generation, J. Mater. Chem. A, 8 (2020), pp. 11665-11673.
[78] X. Li, W. Xu, M. Tang, L. Zhou, B. Zhu, S. Zhu, J. Zhu, Graphene oxide-based efficient and scalable solar desalination under one sun with a confined 2D water path, Proc. Natl. Acad. Sci. U.S.A., 113 (2016), pp. 13953-13958.
[79] Z. Chen, B. Dang, X. Luo, W. Li, J. Li, H. Yu, S. Liu, S. Li, Deep eutectic solvent-assisted in situ wood delignification: A promising strategy to enhance the efficiency of wood-based solar steam generation devices, ACS Appl. Mater. Interfaces, 11 (2019), pp. 26032-26037.
[80] J. Li, X. Zhou, J. Zhang, C. Liu, F. Wang, Y. Zhao, H. Sun, Z. Zhu, W. Liang, A. Li, Migration crystallization device based on biomass photothermal materials for efficient salt-rejection solar steam generation, ACS Appl. Energy Mater., 3 (2020), pp. 3024-3032.
[81] S. He, C. Chen, Y. Kuang, R. Mi, Y. Liu, Y. Pei, W. Kong, W. Gan, H. Xie, E. Hitz, Nature-inspired salt resistant bimodal porous solar evaporator for efficient and stable water desalination, Energy Environ. Sci., 12 (2019), pp. 1558-1567.
[82] C. Finnerty, L. Zhang, D.L. Sedlak, K.L. Nelson, B. Mi, Synthetic graphene oxide leaf for solar desalination with zero liquid discharge, Environ. Sci. Technol., 51 (2017), pp. 11701-11709.
[83] Y. Fan, W. Bai, P. Mu, Y. Su, Z. Zhu, H. Sun, W. Liang, A. Li, Conductively monolithic polypyrrole 3-D porous architecture with micron-sized channels as superior salt-resistant solar steam generators, Sol. Energy Mater. Sol. Cell., 206 (2020), p. 110347.
[84] Y. Xia, Q. Hou, H. Jubaer, Y. Li, Y. Kang, S. Yuan, H. Liu, M.W. Woo, L. Zhang, L. Gao, Spatially isolating salt crystallisation from water evaporation for continuous solar steam generation and salt harvesting, Energy Environ. Sci., 12 (2019), pp. 1840-1847.
[85] J. Zhao, Y. Yang, C. Yang, Y. Tian, Y. Han, J. Liu, X. Yin, W. Que, A hydrophobic surface enabled salt-blocking 2D Ti_3C_2 MXene membrane for efficient and stable solar desalination, J. Mater. Chem. A, 6 (2018), pp. 16196-16204.
[86] L. Zhao, Q. Yang, W. Guo, H. Liu, T. Ma, F. Qu, $Co_{2.67}S_4$-based photothermal membrane with high mechanical properties for efficient solar water evaporation and photothermal antibacterial applications, ACS Appl. Mater. Interfaces, 11 (2019), pp. 20820-20827.
[87] W. Xu, X. Hu, S. Zhuang, Y. Wang, X. Li, L. Zhou, S. Zhu, J. Zhu, Flexible and salt resistant Janus absorbers by electrospinning for stable and efficient solar desalination, Adv. Energy Mater., 8 (2018), p. 1702884.
[88] L. Li, L. Zang, S. Zhang, T. Dou, X. Han, D. Zhao, Y. Zhang, L. Sun, Y. Zhang, GO/CNT-silica Janus nanofibrous membrane for solar-driven interfacial steam generation and desalination, J. Taiwan Inst. Chem. Eng., 111 (2020), pp. 191-197.
[89] Y. Kuang, C. Chen, S. He, E.M. Hitz, Y. Wang, W. Gan, R. Mi, L. Hu, A high-performance self-regenerating solar evaporator for continuous water desalination, Adv. Mater., 31 (2019), p. 1900498.

[90] F. Wang, D. Wei, Y. Li, T. Chen, P. Mu, H. Sun, Z. Zhu, W. Liang, A. Li, Chitosan/reduced graphene oxide-modified spacer fabric as a salt-resistant solar absorber for efficient solar steam generation, J. Mater. Chem. A, 7 (2019), pp. 18311-18317.
[91] Y. Guo, H. Lu, F. Zhao, X. Zhou, W. Shi, G. Yu, Biomass-derived hybrid hydrogel evaporators for cost-effective solar water purification, Adv. Mater., 32 (2020), p. 1907061.
[92] Y. Bian, Q. Du, K. Tang, Y. Shen, L. Hao, D. Zhou, X. Wang, Z. Xu, H. Zhang, L. Zhao, Carbonized bamboos as excellent 3D solar vapor-generation devices, Adv. Mater. Technol., 4 (2019), p. 1800593.
[93] J. Zhang, Y. Yang, J. Zhao, Z. Dai, W. Liu, C. Chen, S. Gao, D. Golosov, S. Zavadski, S. Melnikov, Shape tailored Cu_2ZnSnS_4 nanosheet aggregates for high efficiency solar desalination, Mater. Res. Bull., 118 (2019), p. 110529.
[94] F. Wang, Y. Su, Y. Li, D. Wei, H. Sun, Z. Zhu, W. Liang, A. Li, Salt-resistant photothermal materials based on monolithic porous ionic polymers for efficient solar steam generation, ACS Appl. Energy Mater., 3 (2020), pp. 8746-8754.
[95] C. Jia, Y. Li, Z. Yang, G. Chen, Y. Yao, F. Jiang, Y. Kuang, G. Pastel, H. Xie, B. Yang, Rich mesostructures derived from natural woods for solar steam generation, Joule, 1 (2017), pp. 588-599.
[96] R. Amen, H. Bashir, I. Bibi, S.M. Shaheen, N.K. Niazi, M. Shahid, M.M. Hussain, V. Antoniadis, M.B. Shakoor, S.G. Al-Solaimani, A critical review on arsenic removal from water using biochar-based sorbents: The significance of modification and redox reactions, Chem. Eng. J., (2020), p. 125195.
[97] H.-Y. Zhao, J. Zhou, Z.-L. Yu, L.-F. Chen, H.-J. Zhan, H.-W. Zhu, J. Huang, L.-A. Shi, S.-H. Yu, Lotus-inspired evaporator with Janus wettability and bimodal pores for solar steam generation, Cell Rep. Phys. Sci., (2020), p. 100074.
[98] Y. Long, S. Huang, H. Yi, J. Chen, J. Wu, Q. Liao, H. Liang, H. Cui, S. Ruan, Y.-J. Zeng, Carrot-inspired solar thermal evaporator, J. Mater. Chem. A, 7 (2019), pp. 26911-26916.
[99] K.-K. Liu, Q. Jiang, S. Tadepalli, R. Raliya, P. Biswas, R.R. Naik, S. Singamaneni, Wood–graphene oxide composite for highly efficient solar steam generation and desalination, ACS Appl. Mater. Interfaces, 9 (2017), pp. 7675-7681.
[100] D.P. Storer, J.L. Phelps, X. Wu, G. Owens, N.I. Khan, H. Xu, Graphene and rice-straw-fiber-based 3D photothermal aerogels for highly efficient solar evaporation, ACS Appl. Mater. Interfaces, 12 (2020), pp. 15279-15287.
[101] W. Feast, J. Tsibouklis, K. Pouwer, L. Groenendaal, E. Meijer, Synthesis, processing and material properties of conjugated polymers, Polymer, 37 (1996), pp. 5017-5047.
[102] L. Xu, L. Cheng, C. Wang, R. Peng, Z. Liu, Conjugated polymers for photothermal therapy of cancer, Polym. Chem., 5 (2014), pp. 1573-1580.
[103] Y. Wang, S. Li, P. Zhang, H. Bai, L. Feng, F. Lv, L. Liu, S. Wang, Photothermal-responsive conjugated polymer nanoparticles for remote control of gene expression in living cells, Adv. Mater., 30 (2018), p. 1705418.
[104] Y. Lyu, C. Xie, S.A. Chechetka, E. Miyako, K. Pu, Semiconducting polymer nanobioconjugates for targeted photothermal activation of neurons, J. Am. Chem. Soc., 138 (2016), pp. 9049-9052.
[105] J. Geng, C. Sun, J. Liu, L.D. Liao, Y. Yuan, N. Thakor, J. Wang, B. Liu, Biocompatible conjugated polymer nanoparticles for efficient photothermal tumor therapy, Small, 11 (2015), pp. 1603-1610.
[106] C. Zhang, P. Xiao, F. Ni, L. Yan, Q. Liu, D. Zhang, J. Gu, W. Wang, T. Chen, Converting pomelo peel into eco-friendly and low-consumption photothermic biomass sponge toward multifunctioal solar-to-heat conversion, ACS Sustain. Chem. Eng., 8 (2020), pp. 5328-5337.

[107] C. Xiao, L. Chen, P. Mu, J. Jia, H. Sun, Z. Zhu, W. Liang, A. Li, Sugarcane-based photothermal materials for efficient solar steam generation, ChemistrySelect, 4 (2019), pp. 7891-7895.
[108] X. Wu, G.Y. Chen, W. Zhang, X. Liu, H. Xu, A plant-transpiration-process-inspired strategy for highly efficient solar evaporation, Adv. Sustain. Sys., 1 (2017) , p. 1700046.
[109] Y. Liu, Z. Liu, Q. Huang, X. Liang, X. Zhou, H. Fu, Q. Wu, J. Zhang, W. Xie, A high-absorption and self-driven salt-resistant black gold nanoparticle-deposited sponge for highly efficient, salt-free, and long-term durable solar desalination, J. Mater. Chem. A, 7 (2019), pp. 2581-2588.
[110] S. Chen, Z. Sun, W. Xiang, C. Shen, Z. Wang, X. Jia, J. Sun, C.-J. Liu, Plasmonic wooden flower for highly efficient solar vapor generation, Nano Energy, 76 (2020) 104998.
[111] L. Zhu, M. Gao, C.K.N. Peh, G.W. Ho, Solar-driven photothermal nanostructured materials designs and prerequisites for evaporation and catalysis applications, Mater. Horiz., 5 (2018), pp. 323-343.
[112] S. Cao, Q. Jiang, X. Wu, D. Ghim, H.G. Derami, P.-I. Chou, Y.-S. Jun, S. Singamaneni, Advances in solar evaporator materials for freshwater generation, J. Mater. Chem. A, 7 (2019), pp. 24092-24123.
[113] F. Zhao, Y. Guo, X. Zhou, W. Shi, G. Yu, Materials for solar-powered water evaporation, Nat. Rev. Mater., (2020), pp. 1-14.
[114] T. Chen, Z. Wu, Z. Liu, J.T. Aladejana, X. Wang, M. Niu, Q. Wei, Y. Xie, Hierarchical porous aluminophosphate-treated wood for high-efficiency solar steam generation, ACS Appl. Mater. Interfaces, 12 (2020), pp. 19511-19518.
[115] P.-F. Liu, L. Miao, Z. Deng, J. Zhou, H. Su, L. Sun, S. Tanemura, W. Cao, F. Jiang, L.-D. Zhao, A mimetic transpiration system for record high conversion efficiency in solar steam generator under one-sun, Mater. Today Energy, 8 (2018), pp. 166-173.
[116] H.-Y. Zhao, J. Zhou, Z.-L. Yu, L.-F. Chen, H.-J. Zhan, H.-W. Zhu, J. Huang, L.-A. Shi, S.-H. Yu, Lotus-inspired evaporator with Janus wettability and bimodal pores for solar steam generation, Cell Rep. Phys. Sci., 1 (2020), p. 100074.
[117] F. Liu, B. Zhao, W. Wu, H. Yang, Y. Ning, Y. Lai, R. Bradley, Low cost, robust, environmentally friendly geopolymer–mesoporous carbon composites for efficient solar powered steam generation, Adv. Funct. Mater., 28 (2018), p. 1803266.
[118] Y. Wang, H. Liu, C. Chen, Y. Kuang, J. Song, H. Xie, C. Jia, S. Kronthal, X. Xu, S. He, All natural, high efficient groundwater extraction via solar steam/vapor generation, Adv. Sustain. Sys., 3 (2019), p. 1800055.
[119] H. Gao, M. Yang, B. Dang, X. Luo, S. Liu, S. Li, Z. Chen, J. Li, Natural phenolic compound–iron complexes: sustainable solar absorbers for wood-based solar steam generation devices, RSC Adv., 10 (2020), pp. 1152-1158.
[120] X.-F. Zhang, Z. Wang, L. Song, Y. Feng, J. Yao, Chinese ink enabled wood evaporator for continuous water desalination, Desalination, 496 (2020), p. 114727.
[121] C. Xiao, L. Chen, P. Mu, J. Jia, H. Sun, Z. Zhu, W. Liang, A. Li, Sugarcane-based photothermal materials for efficient solar steam generation, ChemistrySelect, 4 (2019), pp. 7891-7895.
[122] D. Guo, X. Yang, Highly efficient solar steam generation of low cost TiN/bio-carbon foam, Sci. China Mater., 62 (2019), pp. 711-718.
[123] Z. Li, M. Zheng, N. Wei, Y. Lin, W. Chu, R. Xu, H. Wang, J. Tian, H. Cui, Broadband-absorbing WO_{3-x} nanorod-decorated wood evaporator for highly efficient solar-driven interfacial steam generation, Sol. Energy Mater. Sol. Cell., 205 (2020), p. 110254.
[124] J. Xu, F. Xu, M. Qian, Z. Li, P. Sun, Z. Hong, F. Huang, Copper nanodot-embedded graphene urchins of nearly full-spectrum solar absorption and extraordinary solar desalination, Nano Energy, 53 (2018), pp. 425-431.